NASA Reference Publication 1376
Volume III

Clouds and the Earth's Radiant Energy System (CERES) Algorithm Theoretical Basis Document

Volume III—Cloud Analyses and Determination of Improved Top of Atmosphere Fluxes (Subsystem 4)

CERES Science Team
Langley Research Center • Hampton, Virginia

National Aeronautics and Space Administration
Langley Research Center • Hampton, Virginia 23681-0001

December 1995

Available electronically at the following URL address: http://techreports.larc.nasa.gov/ltrs/ltrs.html

Printed copies available from the following:

NASA Center for AeroSpace Information
800 Elkridge Landing Road
Linthicum Heights, MD 21090-2934
(301) 621-0390

National Technical Information Service (NTIS)
5285 Port Royal Road
Springfield, VA 22161-2171
(703) 487-4650

Contents

Preface

The Release-1 CERES Algorithm Theoretical Basis Document (ATBD) is a compilation of the techniques and processes that constitute the prototype data analysis scheme for the Clouds and the Earth's Radiant Energy System (CERES), a key component of NASA's Mission to Planet Earth. The scientific bases for this project and the methodologies used in the data analysis system are also explained in the ATBD. The CERES ATBD comprises 11 subsystems of various sizes and complexities. The ATBD for each subsystem has been reviewed by three or four independently selected university, NASA, and NOAA scientists. In addition to the written reviews, each subsystem ATBD was reviewed during oral presentations given to a six-member scientific peer review panel at Goddard Space Flight Center during May 1994. Both sets of reviews, oral and written, determined that the CERES ATBD was sufficiently mature for use in providing archived Earth Observing System (EOS) data products. The CERES Science Team completed revisions of the ATBD to satisfy all reviewer comments. Because the Release-1 CERES ATBD will serve as the reference for all of the initial CERES data analysis algorithms and product generation, it is published here as a NASA Reference Publication.

Due to its extreme length, this NASA Reference Publication comprises four volumes that divide the CERES ATBD at natural break points between particular subsystems. These four volumes are

I: Overviews
- CERES Algorithm Overview
- Subsystem 0. CERES Data Processing System Objectives and Architecture

II: Geolocation, Calibration, and ERBE-Like Analyses
- Subsystem 1.0. Instrument Geolocate and Calibrate Earth Radiances
- Subsystem 2.0. ERBE-Like Inversion to Instantaneous TOA and Surface Fluxes
- Subsystem 3.0. ERBE-Like Averaging to Monthly TOA

III: Cloud Analyses and Determination of Improved Top of Atmosphere Fluxes
- Subsystem 4.0. Overview of Cloud Retrieval and Radiative Flux Inversion
- Subsystem 4.1. Imager Clear-Sky Determination and Cloud Detection
- Subsystem 4.2. Imager Cloud Height Determination
- Subsystem 4.3. Cloud Optical Property Retrieval
- Subsystem 4.4. Convolution of Imager Cloud Properties With CERES Footprint Point Spread Function
- Subsystem 4.5. CERES Inversion to Instantaneous TOA Fluxes
- Subsystem 4.6. Empirical Estimates of Shortwave and Longwave Surface Radiation Budget Involving CERES Measurements

IV: Determination of Surface and Atmosphere Fluxes and Temporally and Spatially Averaged Products
- Subsystem 5.0. Compute Surface and Atmospheric Fluxes
- Subsystem 6.0. Grid Single Satellite Fluxes and Clouds and Compute Spatial Averages
- Subsystem 7.0. Time Interpolation and Synoptic Flux Computation for Single and Multiple Satellites
- Subsystem 8.0. Monthly Regional, Zonal, and Global Radiation Fluxes and Cloud Properties
- Subsystem 9.0. Grid TOA and Surface Fluxes for Instantaneous Surface Product
- Subsystem 10.0. Monthly Regional TOA and Surface Radiation Budget
- Subsystem 11.0. Update Clear Reflectance, Temperature History (CHR)
- Subsystem 12.0. Regrid Humidity and Temperature Fields

The CERES Science Team serves as the editor for the entire document. A complete list of Science Team members is given below. Different groups of individuals prepared the various subsections that constitute the CERES ATBD. Thus, references to a particular subsection of the ATBD should specify the subsection number, authors, and page numbers. Questions regarding the content of a given subsection should be directed to the appropriate first or second author. No attempt was made to make the overall document stylistically consistent.

The CERES Science Team is an international group led by 2 principal investigators and 19 coinvestigators. The team members and their institutions are listed below.

CERES Science Team

Bruce A. Wielicki, Interdisciplinary Principal Investigator
Bruce R. Barkstrom, Instrument Principal Investigator

Atmospheric Sciences Division
NASA Langley Research Center
Hampton, Virginia 23681-0001

Coinvestigators

Bryan A. Baum
Atmospheric Sciences Division
NASA Langley Research Center
Hampton, Virginia 23681-0001

Maurice Blackmon
Climate Research Division
NOAA Research Laboratory
Boulder, Colorado 80303

Robert D. Cess
Institute for Terrestrial & Planetary Atmospheres
Marine Sciences Research Center
State University of New York
Stony Brook, New York 11794-5000

Thomas P. Charlock
Atmospheric Sciences Division
NASA Langley Research Division
Hampton, Virginia 23681-0001

James A. Coakley
Oregon State University
Department of Atmospheric Sciences
Corvallis, Oregon 97331-2209

Dominique A. Crommelynck
Institute Royal Meteorologique
B-1180 Bruxelles
Belgium

Richard N. Green
Atmospheric Sciences Division
NASA Langley Research Center
Hampton, Virginia 23681-0001

Robert Kandel
Laboratoire de Meteorologie Dynamique
Ecole Polytechnique
91128 Palaiseau
France

Michael D. King
Goddard Space Flight Center
Greenbelt, Maryland 20771

Robert B. Lee III
Atmospheric Sciences Division
NASA Langley Research Center
Hampton, Virginia 23681-0001

A. James Miller
NOAA/NWS
5200 Auth Road
Camp Springs, Maryland 20233

Patrick Minnis
Atmospheric Sciences Division
NASA Langley Research Center
Hampton, Virginia 23681-0001

Veerabhadran Ramanathan
Scripps Institution of Oceanography
University of California-San Diego
La Jolla, California 92093-0239

David R. Randall
Colorado State University
Department of Atmospheric Science
Foothills Campus, Laporte Avenue
Fort Collins, Colorado 80523

G. Louis Smith
Atmospheric Sciences Division
NASA Langley Research Center
Hampton, Virginia 23681-0001

Larry L. Stowe
NOAA/NWS
5200 Auth Road
Camp Springs, Maryland 20233

Ronald M. Welch
South Dakota School of Mines and Technology
Institute of Atmospheric Sciences
Rapid City, South Dakota 57701-3995

Nomenclature

Acronyms

ADEOS	Advanced Earth Observing System
ADM	Angular Distribution Model
AIRS	Atmospheric Infrared Sounder (EOS-AM)
AMSU	Advanced Microwave Sounding Unit (EOS-PM)
APD	Aerosol Profile Data
APID	Application Identifier
ARESE	ARM Enhanced Shortwave Experiment
ARM	Atmospheric Radiation Measurement
ASOS	Automated Surface Observing Sites
ASTER	Advanced Spaceborne Thermal Emission and Reflection Radiometer
ASTEX	Atlantic Stratocumulus Transition Experiment
ASTR	Atmospheric Structures
ATBD	Algorithm Theoretical Basis Document
AVG	Monthly Regional, Average Radiative Fluxes and Clouds (CERES Archival Data Product)
AVHRR	Advanced Very High Resolution Radiometer
BDS	Bidirectional Scan (CERES Archival Data Product)
BRIE	Best Regional Integral Estimate
BSRN	Baseline Surface Radiation Network
BTD	Brightness Temperature Difference(s)
CCD	Charge Coupled Device
CCSDS	Consultative Committee for Space Data Systems
CEPEX	Central Equatorial Pacific Experiment
CERES	Clouds and the Earth’s Radiant Energy System
CID	Cloud Imager Data
CLAVR	Clouds from AVHRR
CLS	Constrained Least Squares
COPRS	Cloud Optical Property Retrieval System
CPR	Cloud Profiling Radar
CRH	Clear Reflectance, Temperature History (CERES Archival Data Product)
CRS	Single Satellite CERES Footprint, Radiative Fluxes and Clouds (CERES Archival Data Product)
DAAC	Distributed Active Archive Center
DAC	Digital-Analog Converter
DB	Database
DFD	Data Flow Diagram
DLF	Downward Longwave Flux

DMSP	Defense Meteorological Satellite Program
EADM	ERBE-Like Albedo Directional Model (CERES Input Data Product)
ECA	Earth Central Angle
ECLIPS	Experimental Cloud Lidar Pilot Study
ECMWF	European Centre for Medium-Range Weather Forecasts
EDDB	ERBE-Like Daily Data Base (CERES Archival Data Product)
EID9	ERBE-Like Internal Data Product 9 (CERES Internal Data Product)
EOS	Earth Observing System
EOSDIS	Earth Observing System Data Information System
EOS-AM	EOS Morning Crossing Mission
EOS-PM	EOS Afternoon Crossing Mission
ENSO	El Niño/Southern Oscillation
ENVISAT	Environmental Satellite
EPHANC	Ephemeris and Ancillary (CERES Input Data Product)
ERB	Earth Radiation Budget
ERBE	Earth Radiation Budget Experiment
ERBS	Earth Radiation Budget Satellite
ESA	European Space Agency
ES4	ERBE-Like S4 Data Product (CERES Archival Data Product)
ES4G	ERBE-Like S4G Data Product (CERES Archival Data Product)
ES8	ERBE-Like S8 Data Product (CERES Archival Data Product)
ES9	ERBE-Like S9 Data Product (CERES Archival Data Product)
FLOP	Floating Point Operation
FIRE	First ISCCP Regional Experiment
FIRE II IFO	First ISCCP Regional Experiment II Intensive Field Observations
FOV	Field of View
FSW	Hourly Gridded Single Satellite Fluxes and Clouds (CERES Archival Data Product)
FTM	Functional Test Model
GAC	Global Area Coverage (AVHRR data mode)
GAP	Gridded Atmospheric Product (CERES Input Data Product)
GCIP	GEWEX Continental-Phase International Project
GCM	General Circulation Model
GEBA	Global Energy Balance Archive
GEO	ISSCP Radiances (CERES Input Data Product)
GEWEX	Global Energy and Water Cycle Experiment
GLAS	Geoscience Laser Altimetry System
GMS	Geostationary Meteorological Satellite
GOES	Geostationary Operational Environmental Satellite
HBTM	Hybrid Bispectral Threshold Method

HIRS	High-Resolution Infrared Radiation Sounder
HIS	High-Resolution Interferometer Sounder
ICM	Internal Calibration Module
ICRCCM	Intercomparison of Radiation Codes in Climate Models
ID	Identification
IEEE	Institute of Electrical and Electronics Engineers
IES	Instrument Earth Scans (CERES Internal Data Product)
IFO	Intensive Field Observation
INSAT	Indian Satellite
IOP	Intensive Observing Period
IR	Infrared
IRIS	Infrared Interferometer Spectrometer
ISCCP	International Satellite Cloud Climatology Project
ISS	Integrated Sounding System
IWP	Ice Water Path
LAC	Local Area Coverage (AVHRR data mode)
LaRC	Langley Research Center
LBC	Laser Beam Ceilometer
LBTM	Layer Bispectral Threshold Method
Lidar	Light Detection and Ranging
LITE	Lidar In-Space Technology Experiment
Lowtran 7	Low-Resolution Transmittance (Radiative Transfer Code)
LW	Longwave
LWP	Liquid Water Path
LWRE	Longwave Radiant Excitance
MAM	Mirror Attenuator Mosaic
MC	Mostly Cloudy
MCR	Microwave Cloud Radiometer
METEOSAT	Meteorological Operational Satellite (European)
METSAT	Meteorological Satellite
MFLOP	Million FLOP
MIMR	Multifrequency Imaging Microwave Radiometer
MISR	Multiangle Imaging Spectroradiometer
MLE	Maximum Likelihood Estimate
MOA	Meteorology Ozone and Aerosol
MODIS	Moderate-Resolution Imaging Spectroradiometer
MSMR	Multispectral, multiresolution
MTSA	Monthly Time and Space Averaging
MWH	Microwave Humidity

MWP	Microwave Water Path
NASA	National Aeronautics and Space Administration
NCAR	National Center for Atmospheric Research
NESDIS	National Environmental Satellite, Data, and Information Service
NIR	Near Infrared
NMC	National Meteorological Center
NOAA	National Oceanic and Atmospheric Administration
NWP	Numerical Weather Prediction
OLR	Outgoing Longwave Radiation
OPD	Ozone Profile Data (CERES Input Data Product)
OV	Overcast
PC	Partly Cloudy
POLDER	Polarization of Directionality of Earth's Reflectances
PRT	Platinum Resistance Thermometer
PSF	Point Spread Function
PW	Precipitable Water
RAPS	Rotating Azimuth Plane Scan
RPM	Radiance Pairs Method
RTM	Radiometer Test Model
SAB	Sorting by Angular Bins
SAGE	Stratospheric Aerosol and Gas Experiment
SARB	Surface and Atmospheric Radiation Budget Working Group
SDCD	Solar Distance Correction and Declination
SFC	Hourly Gridded Single Satellite TOA and Surface Fluxes (CERES Archival Data Product)
SHEBA	Surface Heat Budget in the Arctic
SPECTRE	Spectral Radiance Experiment
SRB	Surface Radiation Budget
SRBAVG	Surface Radiation Budget Average (CERES Archival Data Product)
SSF	Single Satellite CERES Footprint TOA and Surface Fluxes, Clouds
SSMI	Special Sensor Microwave Imager
SST	Sea Surface Temperature
SURFMAP	Surface Properties and Maps (CERES Input Product)
SW	Shortwave
SWICS	Shortwave Internal Calibration Source
SWRE	Shortwave Radiant Excitance
SYN	Synoptic Radiative Fluxes and Clouds (CERES Archival Data Product)
SZA	Solar Zenith Angle
THIR	Temperature/Humidity Infrared Radiometer (Nimbus)

TIROS	Television Infrared Observation Satellite
TISA	Time Interpolation and Spatial Averaging Working Group
TMI	TRMM Microwave Imager
TOA	Top of the Atmosphere
TOGA	Tropical Ocean Global Atmosphere
TOMS	Total Ozone Mapping Spectrometer
TOVS	TIROS Operational Vertical Sounder
TRMM	Tropical Rainfall Measuring Mission
TSA	Time-Space Averaging
UAV	Unmanned Aerospace Vehicle
UT	Universal Time
UTC	Universal Time Code
VAS	VISSR Atmospheric Sounder (GOES)
VIRS	Visible Infrared Scanner
VISSR	Visible and Infrared Spin Scan Radiometer
WCRP	World Climate Research Program
WG	Working Group
Win	Window
WN	Window
WMO	World Meteorological Organization
ZAVG	Monthly Zonal and Global Average Radiative Fluxes and Clouds (CERES Archival Data Product)

Symbols

A	atmospheric absorptance
$B_\lambda(T)$	Planck function
C	cloud fractional area coverage
CF_2Cl_2	dichlorofluorocarbon
$CFCl_3$	trichlorofluorocarbon
CH_4	methane
CO_2	carbon dioxide
D	total number of days in the month
D_e	cloud particle equivalent diameter (for ice clouds)
E_o	solar constant or solar irradiance
F	flux
f	fraction
G_a	atmospheric greenhouse effect
g	cloud asymmetry parameter
H_2O	water vapor

I	radiance
i	scene type
m_i	imaginary refractive index
$\hat{N}$	angular momentum vector
N_2O	nitrous oxide
O_3	ozone
P	point spread function
p	pressure
Q_a	absorption efficiency
Q_e	extinction efficiency
Q_s	scattering efficiency
R	anisotropic reflectance factor
r_E	radius of the Earth
r_e	effective cloud droplet radius (for water clouds)
r_h	column-averaged relative humidity
S_o	summed solar incident SW flux
S_o'	integrated solar incident SW flux
T	temperature
T_B	blackbody temperature
t	time or transmittance
W_{liq}	liquid water path
w	precipitable water
$\hat{x}_o$	satellite position at t_o
x, y, z	satellite position vector components
$\dot{x}, \dot{y}, \dot{z}$	satellite velocity vector components
z	altitude
z_{top}	altitude at top of atmosphere
α	albedo or cone angle
β	cross-scan angle
γ	Earth central angle
γ_{at}	along-track angle
γ_{ct}	cross-track angle
δ	along-scan angle
ε	emittance
Θ	colatitude of satellite
θ	viewing zenith angle
θ_o	solar zenith angle
λ	wavelength
μ	viewing zenith angle cosine

μ_o	solar zenith angle cosine
ν	wave number
ρ	bidirectional reflectance
τ	optical depth
$\tau_{aer}(p)$	spectral optical depth profiles of aerosols
$\tau_{H_2O\lambda}(p)$	spectral optical depth profiles of water vapor
$\tau_{O_3}(p)$	spectral optical depth profiles of ozone
Φ	longitude of satellite
ϕ	azimuth angle
$\tilde{\omega}_o$	single-scattering albedo

Subscripts:

c	cloud
cb	cloud base
ce	cloud effective
cld	cloud
cs	clear sky
ct	cloud top
ice	ice water
lc	lower cloud
liq	liquid water
s	surface
uc	upper cloud
λ	spectral wavelength

Units

AU	astronomical unit
cm	centimeter
cm-sec^{-1}	centimeter per second
count	count
day	day, Julian date
deg	degree
deg-sec^{-1}	degree per second
DU	Dobson unit
erg-sec^{-1}	erg per second
fraction	fraction (range of 0–1)
g	gram
g-cm^{-2}	gram per square centimeter
g-g^{-1}	gram per gram
g-m^{-2}	gram per square meter

h	hour
hPa	hectopascal
K	Kelvin
kg	kilogram
kg-m^{-2}	kilogram per square meter
km	kilometer
km-sec^{-1}	kilometer per second
m	meter
mm	millimeter
μm	micrometer, micron
N/A	not applicable, none, unitless, dimensionless
ohm-cm^{-1}	ohm per centimeter
percent	percent (range of 0–100)
rad	radian
rad-sec^{-1}	radian per second
sec	second
sr^{-1}	per steradian
W	watt
W-m^{-2}	watt per square meter
W-m^{-2}sr^{-1}	watt per square meter per steradian
W-m^{-2}sr^{-1}μm^{-1}	watt per square meter per steradian per micrometer

CERES Top Level Data Flow Diagram

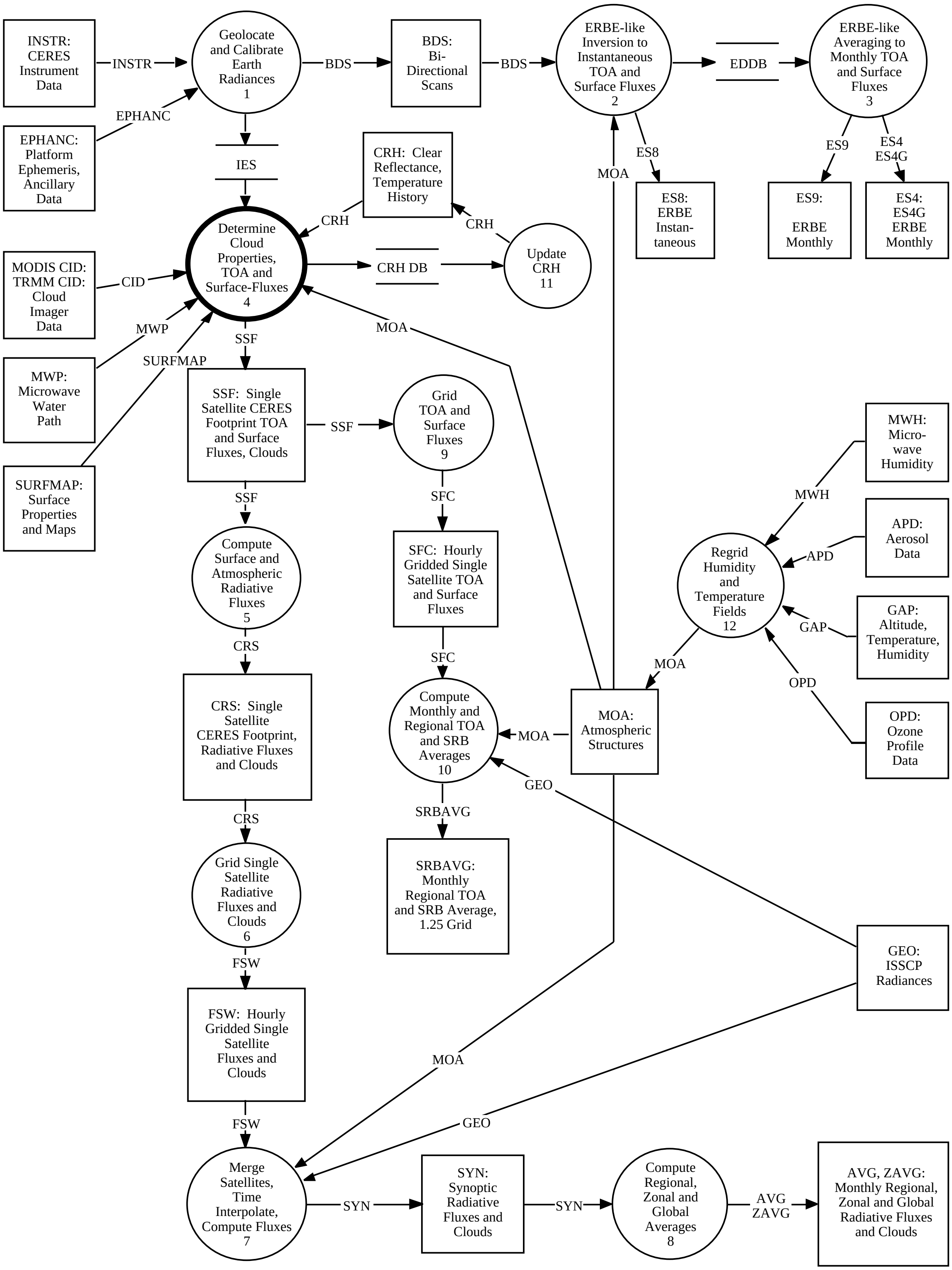

Subsystem 4.0 Top Level Data Flow Diagram

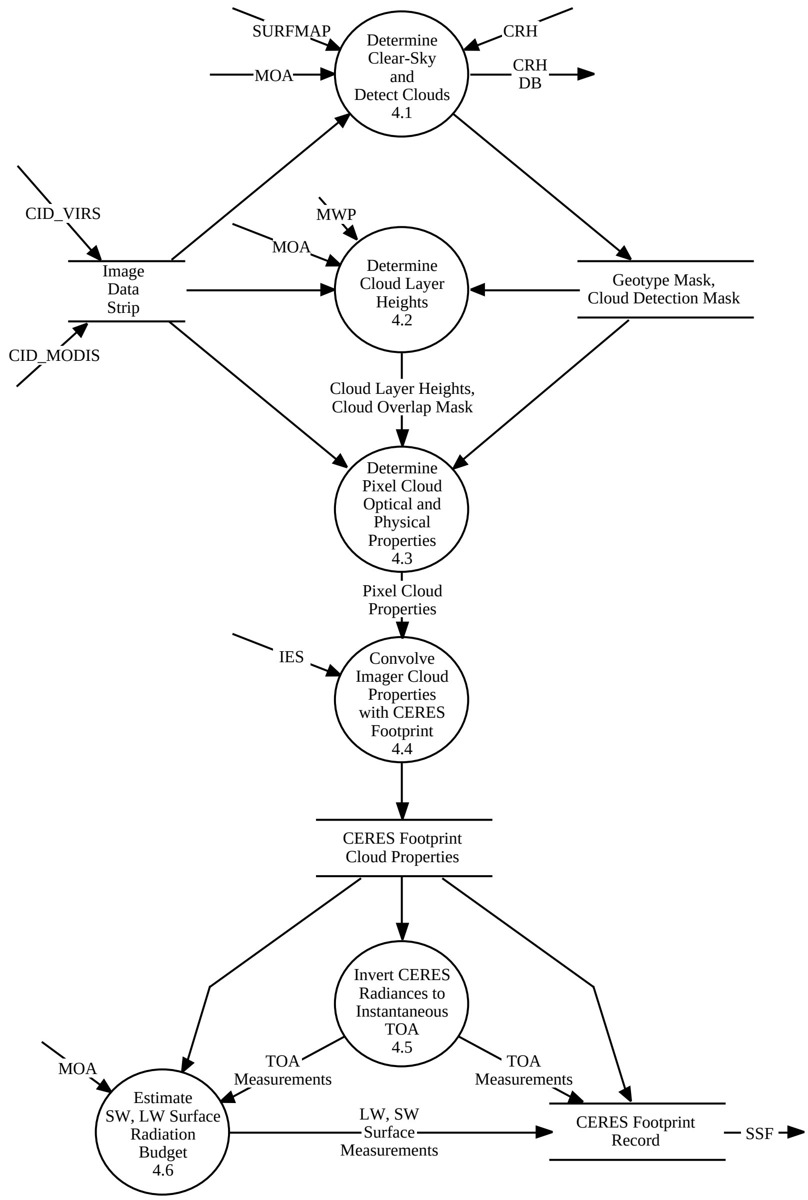

Clouds and the Earth's Radiant Energy System (CERES)

Algorithm Theoretical Basis Document

Overview of Cloud Retrieval and Radiative Flux Inversion

(Subsystem 4.0)

Cloud Working Group Chair

B. A. Wielicki[1]

Inversion Working Group Chair

R. N. Green[1]

Data Management Team

C. J. Tolson[2]
A. Fan[2]

[1]Atmospheric Sciences Division, NASA Langley Research Center, Hampton, Virginia 23681-0001
[2]Science Applications International Corporation (SAIC), Hampton, Virginia 23666

Abstract

One of the major advances of the CERES (Clouds and the Earth's Radiant Energy System) radiation budget analysis over the ERBE (Earth Radiation Budget Experiment) is the ability to use high spectral and spatial resolution cloud imager data to determine cloud and surface properties within the relatively large CERES field of view [20-km diameter for the Earth Observing System (EOS)-AM and EOS-PM, 10 km diameter for TRMM (Tropical Rainfall Measuring Mission)]. For the first launch of the CERES broadband radiometer on TRMM in 1997, CERES will use the VIRS (Visible Infrared Scanner) cloud imager as input. For the next launches on EOS-AM (1998) and EOS-PM (2000), CERES will use the MODIS (Moderate-Resolution Imaging Spectroradiometer) cloud imager data as input.

This overview summarizes the Subsystem 4 CERES algorithms which

1. *Determine clear-sky radiances and detect pixels containing clouds*
2. *Determine well-defined cloud layers and identify multilayer pixels*
3. *Determine cloud properties for each imager pixel*
4. *Map the imager cloud properties to the CERES broadband radiance footprint*
5. *Use the CERES footprint cloud properties to determine an angular distribution model for the conversion of radiance to top-of-atmosphere (TOA) flux*
6. *Use the TOA fluxes and parameterizations to estimate surface radiative fluxes*

Angular sampling errors were determined to be the largest error source for ERBE shortwave fluxes. The increased accuracy of CERES cloud property determination and the new angular models are expected to reduce these errors by a factor of 3 to 4. The cloud properties and radiative fluxes for each CERES footprint are also key to providing more accurate estimates of in-atmosphere radiative fluxes. These in-atmosphere radiative flux calculations are discussed in Subsystem 5.

4.0. Overview of Cloud Retrieval and Radiative Flux Inversion

4.0.1. Introduction

This documentation is intended as an overview of the CERES cloud retrieval algorithm. The cloud retrieval algorithm has two major objectives.

The first objective is to derive surface and cloud properties sufficient to classify a unique set of targets with distinctly different anisotropic radiation fields. This is required so that the CERES rotating azimuth plane scanner can observe a complete range of surface and cloud targets for all typical viewing and solar angle geometries for a given satellite orbital geometry. These cloud determinations are then combined with the CERES broadband scanner radiance data to derive empirical models of shortwave (SW) and longwave (LW) anisotropy required to accurately convert the CERES-measured radiances into unbiased estimates of radiative fluxes. For example, we would combine observations of boundary layer cumulus with cloud fractions between 20 and 30% over a tropical forest background. In turn, this cumulus cloud class might further be broken into several optical depth classes. In this manner, even the potentially large but uncertain effect of 3-D cloud structure can be implicitly included in the anisotropic models. Testing of these concepts has begun by using the Nimbus-7 THIR (Temperature-Humidity Infrared Radiometer) and TOMS (Total Ozone Mapping Spectrometer) cloud properties (Stowe et al. 1988) and ERB (Earth Radiation Budget) broadband radiances (Jacobowitz et al. 1984). The testing will continue with the Release 1 CERES cloud algorithm using AVHRR (Advanced Very High Resolution Radiometer), HIRS (High-Resolution Infrared Sounder), and ERBE global radiance data sets.

The second objective is to provide a set of cloud properties optimally designed for studies of the role of clouds in the Earth's radiation budget. In particular, cloud properties determined using high spatial (0.25–2 km at nadir) and spectral resolution cloud imager data will be matched to each CERES footprint (10–20 km at nadir) to as consistently as possible tie the cloud physical and cloud broadband radiative properties. These cloud properties will be used in calculations of the surface and in-atmosphere radiative fluxes. Because all current cloud remote sensing methods use 1-D radiative transfer models, which are not appropriate for optically thick cumulus clouds, the close tie of CERES TOA fluxes to imager cloud properties allows a first-order correction for 3-D cloud effects. For example, TOA reflected SW flux computed using the 1-D-determined imager cloud optical depth and cloud particle size may differ greatly from the observed TOA flux. The observed flux used empirical models of cloud anisotropy to correctly convert radiance into flux even for 3-D cloud structure. This flux can then be used to determine an "equivalent" plane-parallel cloud optical depth or to specify a 3-D cloud parameter such as cloud aspect ratio. In this sense, the CERES cloud algorithm will produce an initial estimate of cloud properties. This estimate will then be modified to obtain consistency in cloud properties and TOA broadband radiative fluxes. This consistency will be essentially that required to examine global climate models, which use 1-D radiative flux computations similar to those performed by CERES.

4.0.2. Input and Output Data

The primary input data sets for Subsystem 4 are the CERES broadband radiance data and the cloud imager data. Other auxiliary input data sets are discussed more fully in Subsystems 4.1–4.3 and in the input data descriptions in appendix A. The CERES instrument data are described in Subsystem 1. The cloud imager data vary between prelaunch studies, TRMM, and EOS, and a brief overview is given below.

VIRS is a next generation version of the AVHRR scanning radiometer with a 2-km diameter nadir field of view and five spectral channels (0.65, 1.6, 3.75, 10.8, and 12.0 μm). The major advances over the current AVHRR are the addition of a 1.6-μ channel and onboard solar channel calibration. The AVHRR instrument has shown large changes in instrument gain with time (Staylor, 1990; NESDIS, 1993).

MODIS (King et al. 1992) will be a major improvement over both AVHRR and VIRS. Onboard calibration will be greatly improved for solar reflectance channels by including onboard lamps, solar diffuser plate, and the ability to use the moon as a stable target. Channel spectral wavelengths will also be monitored in flight. MODIS provides 11 spectral channels of prime use for cloud analysis, including

- 13.3, 13.6, and 13.9 μm for determining thin cirrus cloud height
- 1.38 μm for detecting very thin cirrus, even in the presence of low cloud
- 3.7, 8.5, 11, and 12 μm for determining nighttime cloud particle size/phase
- 0.65, 1.6, and 2.1 μm for determining daytime optical depth, particle size/phase

The thermal infrared channels have a field of view diameter of 1 km, the near infrared are 0.5 km, and the visible channel is 0.25 km. The high spatial resolution visible channel eliminates the problem of partially cloud filled fields of view even for boundary layer clouds such as cumulus (Wielicki and Parker, 1992).

The CERES cloud retrieval algorithm will use the cloud imager data to produce estimates of basic cloud physical and optical properties within each CERES footprint including

- Fractional coverage
- Temperature/height/pressure
- Optical depth (0.65 µm)
- Emissivity (11 µm)
- Particle size and phase
- Liquid/ice water path
- Vertical thickness
- Vertical aspect ratio

The cloud properties are listed roughly in the order of expected accuracy and current understanding of their retrieval. The first four properties are reasonably well understood, the next two are in advanced stages of development, and the last two are only in the beginning stages of development, and may only provide useful information for a limited range of cloud conditions. These properties cover a reasonably complete set of variables to describe the effect of clouds on the radiative fluxes at the surface, within the atmosphere, and at the top of the atmosphere. They are not a rigorously exhaustive set. For example, cloud vertical aspect ratio is a variable which is intended (along with cloud fraction and cloud optical depth) to allow at least a limited investigation of the effects of 3-D radiative transfer issues.

Surface observers indicate that about half of cloud observations are multilayered (Warren et al. 1985), and that multilayered clouds are much more likely over ocean than land. Over ocean, 52% of all observations are multilayered while 43% are single-layered. Over land, 31% are multilayered while 47% are single-layered. Tian and Curry (1989) used the combined satellite, aircraft, and surface cloud observations in the Air Force 3DNEPH data to examine cloud overlap assumptions over the North Atlantic Ocean, and concluded that for cloud layers within 1 km in altitude, maximum overlap is most accurate, while for cloud altitudes separated by 3 km or more, random overlap is the best assumption. Their study further concluded that at a spatial scale of 45 km (similar to the CERES footprint) 75% of the multilayered cases consisted of two-layer cloud systems. As the spatial scale of interest increases to 220 km, three-layer cases dominate. We conclude that the CERES cloud analysis must commonly address the issue of two-layer cloud systems.

All current global satellite cloud climatologies assume a single cloud layer to occur in each imager pixel, although multiple cloud layers are allowed in large regions. For example, subtropical optically thin cirrus overlying a lower boundary layer cloud gives cloud height properties dominated by the cold cirrus and cloud optical depth dominated by the optically thicker stratus cloud. Recent studies of the sensitivity of the LW surface radiation budget to cloud overlap assumptions show that knowledge of cloud overlap is more important than accurate knowledge of the thickness of individual cloud layers (Subsystem 5.0).

CERES will employ two strategies to improve the remote sensing of multilayer clouds. For an optically thin high cloud over low clouds, the MODIS CO_2 sounding channels will be used to establish the upper cloud height and optical depth, while the spectral window visible and infrared channels will be used for the low clouds (Baum et al. 1994). For an optically thick high cloud over a low cloud, the cloud imager channels will be used for the high cloud properties, while passive microwave liquid water path (LWP) measurement (Greenwald et al. 1993) is used to indicate the presence of the lower cloud layer over ocean backgrounds. These two improvements for sensing multilevel clouds should provide substantially better estimates of LW surface and in-atmosphere radiation budget.

4.0.3. Algorithm Assumptions

Any algorithm to remotely sense physical or radiative properties is based on an assumed physical model. This conceptual model may be explicit (plane-parallel radiative calculations) or implicit (piecewise constant spatial averaging). The more explicit the conceptual model, the more precisely the algorithm strengths and weaknesses can be understood. This is particularly the case in validating the algorithm results. The most fruitful validation is not simply the comparison of end results, but rather the validation of underlying assumptions. The successes and failures of these assumptions lead to critical new results and methods.

The CERES cloud identification and radiative flux determination algorithms are based on the following assumptions.

1. ***Cloud-filled pixel assumption: Clouds are much larger than a cloud imager pixel, so that cloud cover in a pixel is 0 or 1.***

This assumption is the subject of much debate. While no data have conclusively answered this question, initial answers are beginning to arrive. The cloud types most subject to error are those with the smallest cloud cells such as cumulus. Figure 4.0-1 shows the accuracy of detecting oceanic boundary layer cloud amount with different spatial resolution sensors (8, 4, 2, 1, 0.5, and 0.25 km). The results are an extension of the results of Wielicki and Parker (1992) to a much larger number of cases. The results shown here are for 52 cloud fields (each 58.4 km square), but show similar results to those found earlier, although now the bias can be shown to be a systematic function of cloud amount.

Each point in the scatter plot gives the regional cloud fraction in one of the 58.4-km regions. Note that the current ISCCP (International Satellite Cloud Climatology Project) data use 4–8 km resolution data, depending on the satellite [GOES (Geostationary Operational Environmental Satellite) is 8 km, GMS (Geosynchronous Meteorological Satellite) and METEOSAT are 5 km, and AVHRR is 4 km]. Figure 4.0-1 shows that the maximum “beam filling” error is at a cloud amount of 0.5, where partially cloud-filled pixels are sufficiently bright to trigger the cloud threshold, but are treated as cloud filled. For cloud amounts less than about 0.2, the large pixel data underestimate cloud amount, since few of the pixels have sufficient cloud cover to exceed the cloud threshold.

For 8-km data, average cloud fraction for the 52 cases is biased too large by 0.06, with a 1s rms error of about 0.11. The use of AVHRR 4-km data reduces this error by about 30% to 0.04 bias and 0.08 (1s). The VIRS 2-km data have a bias of 0.02 and a 1s of 0.06 (less than half the ISCCP error). The 0.5 km and 0.25 km results typical of MODIS resolution show a small bias of about –0.02 and 1s of 0.04. The bias for these last two cases is dominated by the difference in reflectance threshold between the reference data (Rclr + 1.5%) and the ISCCP radiance threshold, which for the cases here is equivalent to approximately Rclr + 4.5%, where Rclr is the nadir bidirectional reflectance as defined in Wielicki and Parker (1992). Given very high spatial resolution data, the ISCCP threshold misses significant amounts of optically thin clouds, even for boundary layer clouds. Note that for these cases, the reference threshold would detect a cloud with 10- m water droplets at a visible optical depth of about 0.3. If the reflectance threshold of the 0.25-km pixel analysis is set equal to the reference case, the two agree to better than 0.01 in cloud fraction. We conclude that the MODIS 0.25-km visible channel is sufficient to derive cloud cover for oceanic boundary layer clouds with errors of a few percent or less.

Cirrus clouds have also been examined using numerous Landsat scenes. For cirrus, the thermal threshold dominates, so that the MODIS 1-km and VIRS 2-km resolutions are pertinent to the CERES algorithm. Figure 4.0-2 gives a similar result for cirrus cloud fields. As in Wielicki and Parker (1992), the cirrus clouds show very little spatial resolution effects for pixel sizes of 1–8 km. We conclude that the cloud-filled pixel assumption is reasonable for AVHRR, VIRS, and MODIS for cirrus clouds. While these results are encouraging, further work is needed, especially for land cumulus. Studies to verify the accuracy of this approximation are underway using cumulus cloud fields over the Amazon.

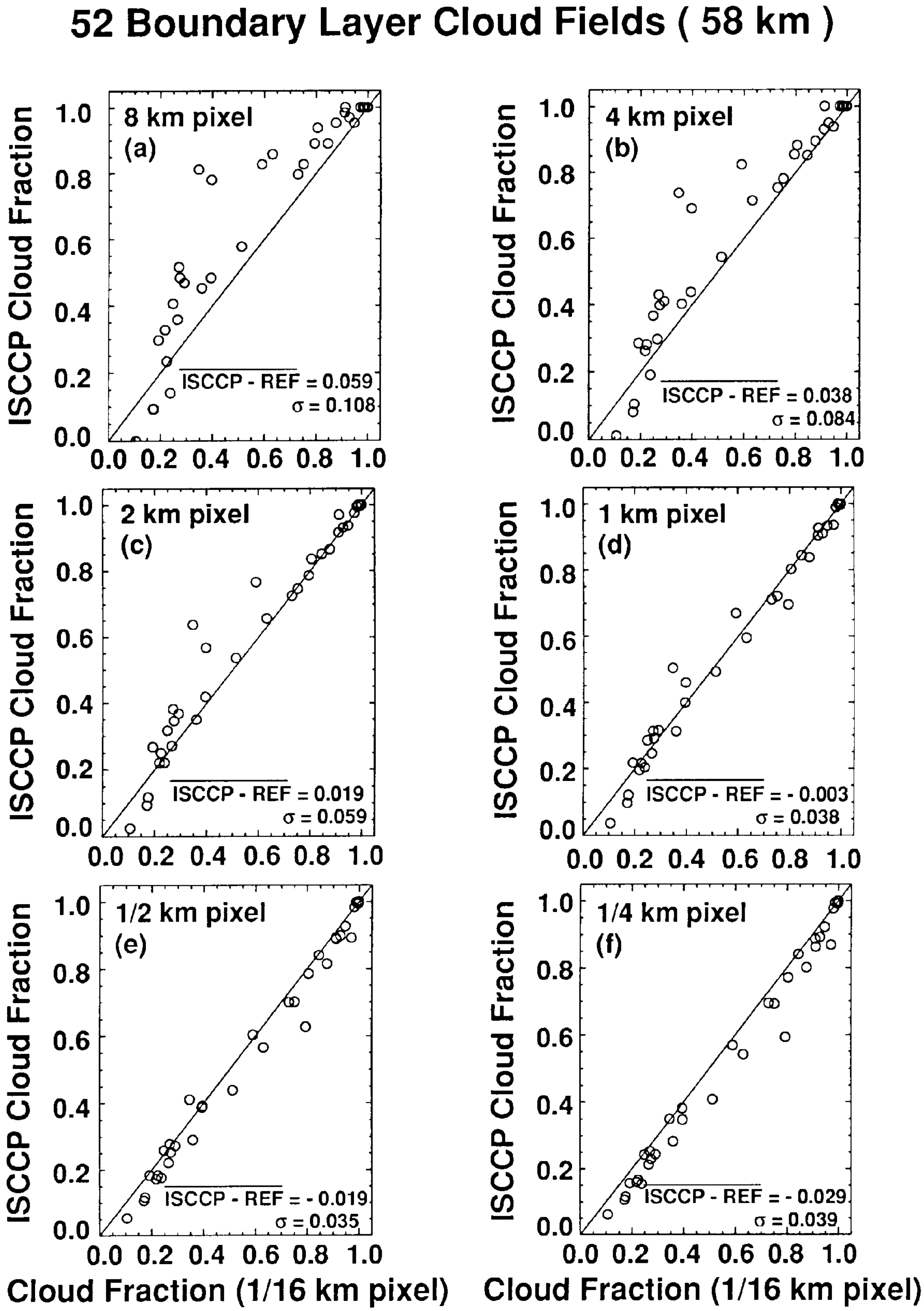

Figure 4.0-1. Effect of sensor spatial resolution on ISCCP threshold estimate of boundary layer cloud fraction. Reference is 57-m spatial resolution Landsat data. Each point represents cloud fraction for a 58-km region.

The most difficult problem may be the detection of boundary layer clouds at night, when even the MODIS retrievals will require the use of 1-km data. The thermal contrast of these clouds at night is much less than the visible reflectance contrast during the day. The problem of missing optically thin clouds may become more severe. Verification of the accuracy of nighttime detection must be performed with coincident lidar and cloud imager data, or with very high spatial resolution data from the MAS (MODIS Airborne Simulator) on the ER-2 aircraft.

CERES will examine the use of spatial coherence to infer subpixel cloud fraction using techniques to correct for emittances less than 1 (Lin and Coakley, 1993). This would allow the Release 2 algorithm to eliminate the cloud-filled pixel assumption for VIRS data and nighttime MODIS data.

2. Independent pixel assumption: Clouds can be modeled as plane-parallel, even though they exhibit large horizontal variability in optical depth.

An excellent discussion of this assumption can be found in Cahalan et al. (1994). They demonstrate that the assumption is accurate to a few percent for narrowband flux calculations with overcast marine boundary layer clouds. Wielicki and Parker (1992) found support for the plane-parallel assumption using Landsat nadir radiances at 0.83 μm and 11 μm for broken and solid boundary layer clouds. Stackhouse and Stephens (1994) found rms errors of up to 20% in derived optical depths using plane-parallel radiance calculations, although bias errors were much smaller. In general, this assumption will be less accurate for radiances than for fluxes.

The relatively small errors of this assumption seem to be caused by three properties of the clouds examined:

- A red spectrum of radiance variability, typical of most meteorological fields. This means that as spatial scale decreases, cloud optical property variability decreases. A red spectrum limits the “sharpness” of cloud edges.
- Low to moderate optical depths for the cirrus and marine boundary layer clouds, especially for broken clouds (Harshvardhan et al. 1994; Wielicki and Parker, 1992; Luo et al. 1994). Welch et al. (1980) used Monte Carlo radiative model calculations to show that the effect of horizontal inhomogeneity on fluxes became pronounced only for cloud optical depths above about 8. Most of the cirrus and broken marine boundary layer clouds appear to be at lower optical depths, thereby minimizing the effects.
- Cloud vertical aspect ratios (vertical/horizontal) are typically much less than 1 for cirrus and inversion-capped boundary layer clouds.

The most severe test of this assumption will come with examination of boundary layer cumulus over land (Wielicki and Welch, 1986), and deep convection over land and ocean, which will have large optical depths and large aspect ratios. One of the complications caused by deep convection, or any high optically thick cloud with sharp edges, is the problem of cloud shadowing. Subsystem 4.3 discusses the effect of shadowing on cloud optical property retrieval and suggests strategies for minimizing the effect.

Even if the independent pixel assumption is without error, Cahalan et al. (1994) and Stephens (1988) showed that optical depths cannot be spatially or temporally averaged without causing large errors in radiative flux calculations. This error is simply caused by the nonlinear relationship between albedo and optical depth. CERES cloud retrievals will minimize this problem by saving 1-D histograms of cloud visible (0.65 μm) optical depth calculated using the highest resolution cloud imager data available (Subsystem 4.5). These histograms will be carried through the spatial gridding and time (t) averaging processes as well as averaging to instantaneous CERES footprints. One step to minimize this error is to average $\ln(t)$ as opposed to a linear average of t (Rossow et al. 1991). The advantage of this process is that cloud spherical albedo is roughly linear in $\ln(t)$, so that this variable comes closer to conserving the cloud albedo. In fact, the errors showed by Cahalan et al. (1994) would have been significantly reduced if this averaging had been used.

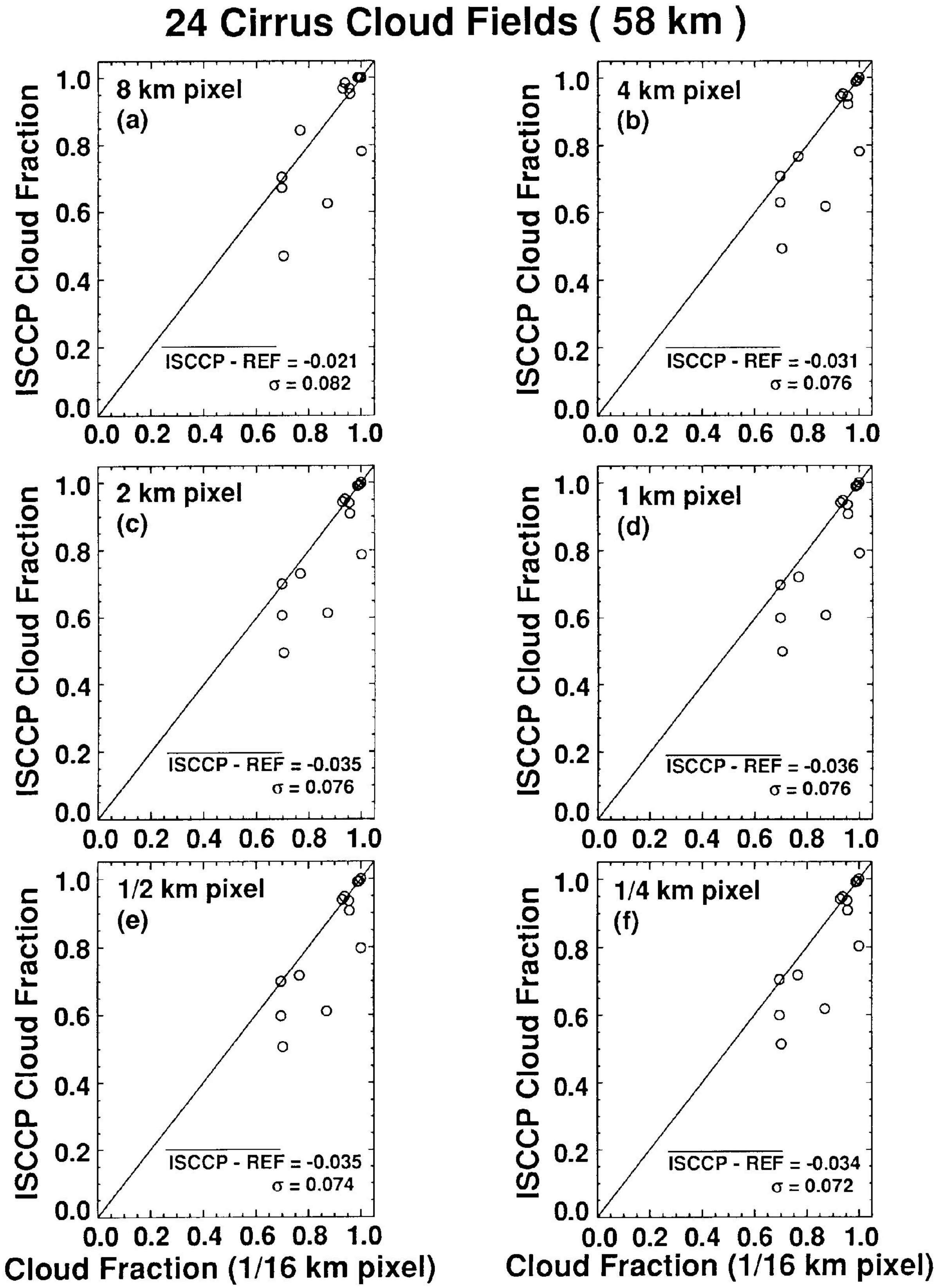

Figure 4.0-2. Effect of sensor spatial resolution on ISCCP threshold estimate of cirrus cloud fraction. Reference is 57-m spatial resolution Landsat data. Each point represents cloud fraction for a single 58-km region over ocean.

Although we discussed the impact of the cloud-filled pixel assumption on cloud fraction, what is its impact on cloud optical depth? Figure 4.0-3 shows the effect of varying pixel size on the derived average optical depth in the 58.4 km region. The results shown are for linear-averaged optical depth, and therefore are more typical of spatially averaged error in LWP which for a fixed cloud particle size is linear in optical depth (Subsystem 4.3). For 8-km pixels, the bias error is an underestimate of 23%, with a 1σ of 25%. The fractional error is much larger than cloud amount errors because both the spatial averaging error discussed above (using a spatially averaged reflectance) will always underestimate the true average optical depth (Cahalan et al. 1994) and the cloud filled-pixel error (clear regions in cloudy pixels lower the mean reflectance) contrive to underestimate the optical depth. For the 2-km VIRS data, the error drops to a bias of 12%, while finally for 0.25-km data, the bias becomes an overestimate of 8% with a 1σ of 12%. Why the overestimate for small pixels? This shows the effect of changing from the reference threshold at Rclr + 1.5% to the ISCCP value of approximately Rclr + 4.5%. The ISCCP threshold misses some of the optically thin clouds picked up by the smaller threshold. This is confirmed by the fact that the bias is largest for the smallest optical depth clouds.

Further studies are needed to examine the errors for logarithmic averaging of optical depth, and the determination of optimal thresholds as a function of spatial resolution. Finally, as discussed by Stephens (1988) and Rossow (1989), the optimal methods for spatial and temporal averaging of cloud physical and optical properties have yet to be established. CERES will perform studies using the broadband radiative models discussed in Subsystem 5 along with imager pixel-level cloud properties to examine the effect of spatial averaging on relationships between cloud properties and optical properties in time- and space-averaged data.

3. ***Cloud height has the smallest horizontal spatial variability, followed by cloud particle phase/size. Finally, cloud visible optical depth has the largest spatial variability.***

If all cloud properties are equally variable in space, then we must treat every cloud imager pixel as a unique cloud retrieval, totally independent of its neighbors. Neighboring pixels in this case do not impart any new information. At best they may be used in larger groups only to decrease the amount of instrument noise.

If, on the other hand, one or more of the cloud properties exhibits much larger spatial scales or less variability than the other cloud properties, then it is possible to group the data and derive additional information from collections of pixels that would not be feasible, or would be ambiguous, using a single pixel. Many cloud algorithms use exactly this assumption, but for different cloud properties. The spatial coherence algorithm (Coakley and Bretherton, 1982) relies on the uniformity of cloud height to derive estimates of overcast cloud layer properties, to separate these overcast pixels from broken cloud or variable emissivity pixels, and to ascribe an effective cloud amount to each variable pixel. Some recent studies of cloud particle size (Lin and Coakley, 1993) further assume that both cloud height and cloud particle size are constant over a distribution of pixels. The method of Arking and Childs (1985) assumed that cloud height and cloud visible optical depth were constant and adjusted cloud amount to achieve a consistent cloud retrieval.

Rigorous proof of these assumptions is not yet available, although for cloud height, the recent availability of ECLIPS (Experimental Cloud Lidar Pilot Study) lidar data for cloud base, and 3-mm radar data from FIRE (First ISCCP Regional Experiment) provide data sets adequate to begin a more thorough examination of this assumption. Uplooking LWP data such as taken during the FIRE experiments can be used to infer the variability of optical depth. We conducted an initial examination of this variability using the 1987 FIRE data from San Nicolas Island for LWP over a 19-day period, and cloud base altitude from ECLIPS lidar for a 5-day period. These initial data confirmed the usual qualitative assumption that cloud height is much less variable. These data sets are too limited to base global analysis on, however, and further work is needed in this area for a wider range of cloud types. The answer is likely to be a function of cloud type and whether cloud base or cloud top is most important. A very

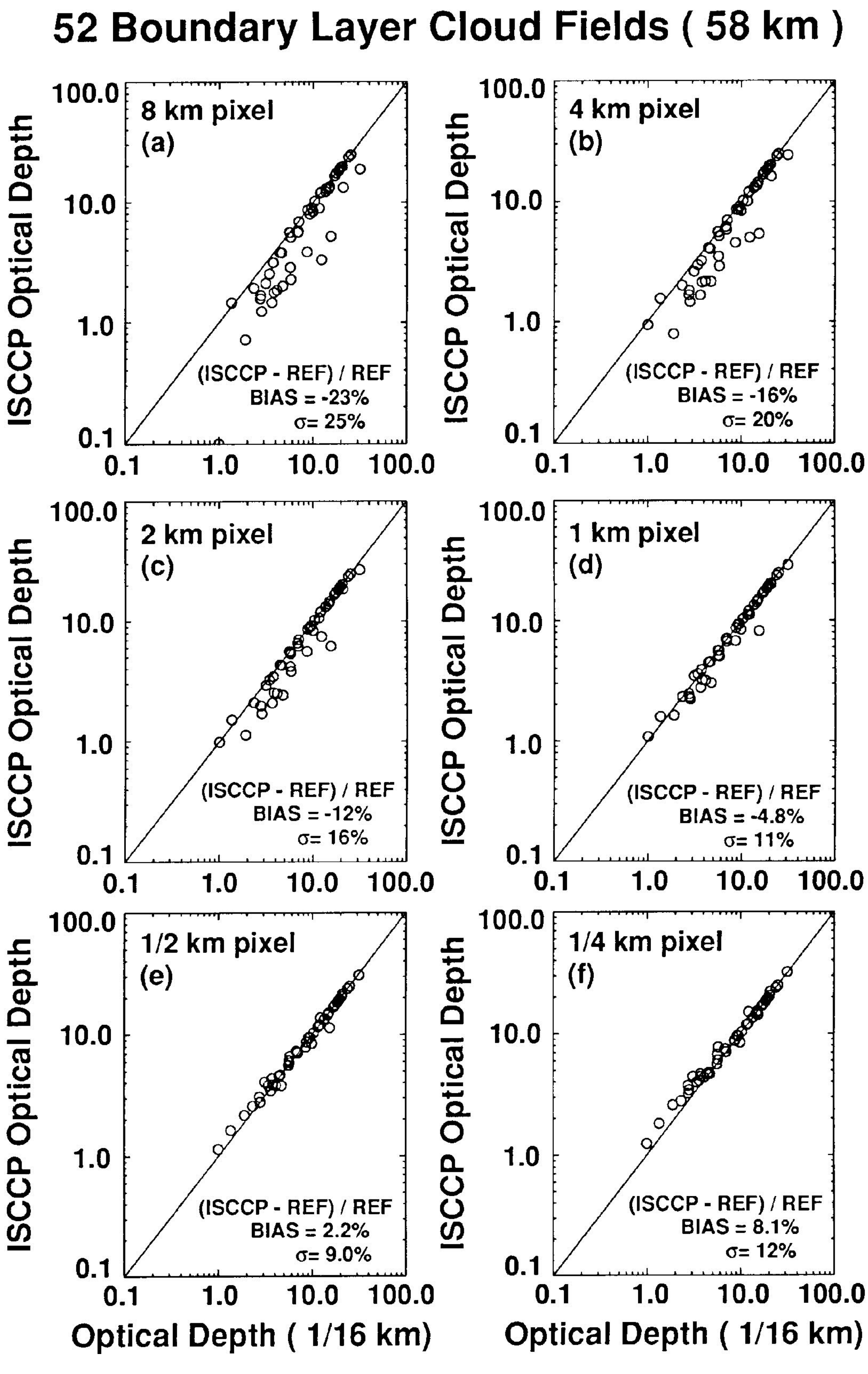

Figure 4.0-3. Effect of sensor spatial resolution on ISCCP-like estimate of cloud optical depth for boundary layer cloud cases. Reference is 57-m spatial resolution Landsat data. Each point is a linear average of optical depth for cloudy pixels in a 58-km region.

interesting data set in this regard is the global lidar data taken from the space shuttle in late 1994 by the Langley Lidar In-Space Technology Experiment (LITE). Other critical future data sets will be long time series from 3-mm radar at ARM (Atmospheric Radiation Measurement) sites in the tropics, mid latitudes, and polar regions. The assumption used here that cloud particle size is more spatially contiguous than visible optical depth is based on aircraft reports that cloud liquid water content seems to vary more with cloud particle number than with cloud particle size. This assumption is also supported by initial analysis of satellite inferred cloud properties using the AVHRR visible channel (optical depth variability) and 3.7-μm channel (cloud particle size) as shown in Coakley et al. (1987) and Coakley and Davies (1986). A rigorous study of this conclusion over a large data set has not been carried out to our knowledge. Much of this data exists, at least for boundary layer clouds, convective clouds, and cirrus.

Given the importance of multilayer clouds to the LW surface radiation balance, and to the in-atmosphere radiative fluxes, the CERES algorithms will begin to address the issue of remote sensing of multilayer cloud systems. One of the key proposals for unscrambling complex cloud overlap cases is to allow cloud height information to propagate horizontally from single-layer to multilayer cloud observations. A key assumption is that the layers are reasonably independent, so that cloud heights in single-layer regions are similar to cloud heights in multilayer overlapped cloud regions. Clearly if the cloud layers are vertically close (1 km or less) they are likely to be strongly correlated. If they are vertically separated by more than 6 km, they are probably poorly correlated (cirrus over boundary layer stratus). An exception to this would obviously be storm fronts, where large systematic cloud height changes occur over several hundred km. As a first approximation, CERES will assume that cloud layers are uncorrelated when separated by more than about 3 km. In Release 1, CERES will only consider the overlap case of nonblack cloud over lower cloud, with the layers separated by at least 3 km. The 3-km separation is also required to get a sufficient signal in the thermal infrared to attempt separation of two cloud layers overlapped in a imager pixel (Baum et al. 1994). Note that variations in the height of nonoverlapped cloud layers can be detected for much smaller changes in cloud height, down to perhaps 0.25 km. The restriction here is for initial attempts to unscramble the signal from an optically thin upper cloud over a lower cloud.

In Release 2, CERES will add the ability over oceans to use passive microwave data to estimate cloud LWP beneath an optically thick ice cloud. For other regions of optically thick high- or middle-level cloud, assumptions must be made about cloud overlap: random, maximum, or minimum overlap. Further discussions of this issue can be found in Hahn et al. (1982) and Tian and Curry (1989). Finally, we assume that no more than two cloud layers are present at the same time. A great deal of work needs to be done on the cloud layering assumptions, and the best data set appears to be the recent field observations using 3-mm or 8-mm cloud radar. There is also an urgent need for a spaceborne cloud radar to achieve global measurements of cloud height and cloud overlap. Cloud lidar will work for some systems, but only if the total cloud optical depth of both layers is less than about 3.

4. Cloud layers separated by more than 3 km in height are independent.

The initial reason for this assumption is to allow the use of nearby single-layer cloud height observations to constrain the solution of optical properties for two-layer cloud overlap conditions. This assumption also enters into how to handle the time and space averaging of cloud overlap conditions. If the layers are independent, then cloud physical and optical properties can be saved in cloud height categories, where cloud properties for an imager pixel are categorized based on the effective cloud pressure, p_e:

High Cloud:	$p_e < 300$ hPa
Upper Middle:	$300 < p_e < 500$ hPa
Lower Middle:	$500 < p_e < 700$ hPa
Low:	$700 < p_e < 1000$ hPa

p_e is the pressure in the atmospheric temperature profile which corresponds to the effective radiating temperature of the cloud. For a thin cloud this is the cloud center; for a thick cloud it is the cloud top. This can be thought of as the radiative center of mass for the cloud as viewed from the TOA in the thermal infrared part of the spectrum. Given the independence of cloud layers, we do not require that separate cloud properties be saved for every overlap combination of two cloud height categories. Instead, we simply save the fraction of space or time covered by each of the 11 cloud overlap conditions:

1. No cloud
2. Low cloud only
3. Lower middle cloud only
4. Upper middle cloud only
5. High cloud only
6. High cloud over upper middle cloud
7. High cloud over lower middle cloud
8. High cloud over low cloud
9. Upper middle cloud over lower middle cloud
10. Upper middle cloud over low cloud
11. Lower middle cloud over low cloud.

The selection of category pressure boundaries is somewhat arbitrary. The current selection is based on the following criteria:

- A minimum of three cloud layers to distinguish major cloud types: high/middle/low clouds
- A pressure boundary at 500 hPa, the level chosen for CERES initial atmospheric radiative flux analysis, thereby separating the troposphere into two parts for radiative heating
- Pressure boundaries which are a subset of those used by ISCCP, so that direct comparisons can be made to the ISCCP data; ISCCP has boundaries which include 680 and 310 hPa
- Maintain a minimum of about 3-km separation between height categories, so that layers are often independent

These criteria led to the selection of four cloud height categories and boundaries at 700, 500, and 300 hPa. In the tropics, the 300-hPa boundary occurs at a temperature of about 240K, similar to the 235K threshold often used to distinguish precipitating clouds. This selection should prove useful when comparing radiative and latent heating profiles estimated using TRMM data.

A schematic diagram summarizing the cloud height categories and layering assumptions is shown in Figure 4.0-4 which is taken from Subsystem 4.4.

5. ***Clouds are sufficiently varied in time and space that there is currently no single cloud algorithm that works well for the all cloud types and cloud properties.***

As is often the case when attacking a formidable problem, each cloud algorithm has commonly examined a small piece of the whole cloud retrieval problem. ISCCP has developed the most complete analysis to date, although the ISCCP algorithm is severely limited by the restriction to use only two spectral bands, a visible and an infrared window channel. The CERES cloud analysis will have a more complete set of measurements to use, including all five of the AVHRR channels, the 1.6-µm channel on VIRS and MODIS, new channels on MODIS, as well as passive microwave data. In spite of this additional information, there is still no single algorithm available to handle the wide diversity of cloud properties observed over the globe. Instead, a robust cloud analysis which gains the best information from each spectral channel and instrument will by nature be forced to combine multiple cloud algorithms.

Clear and accurate combination of diverse algorithms is a difficult task. In order to achieve this strategy, CERES has a team which includes experts in many of these different approaches. This

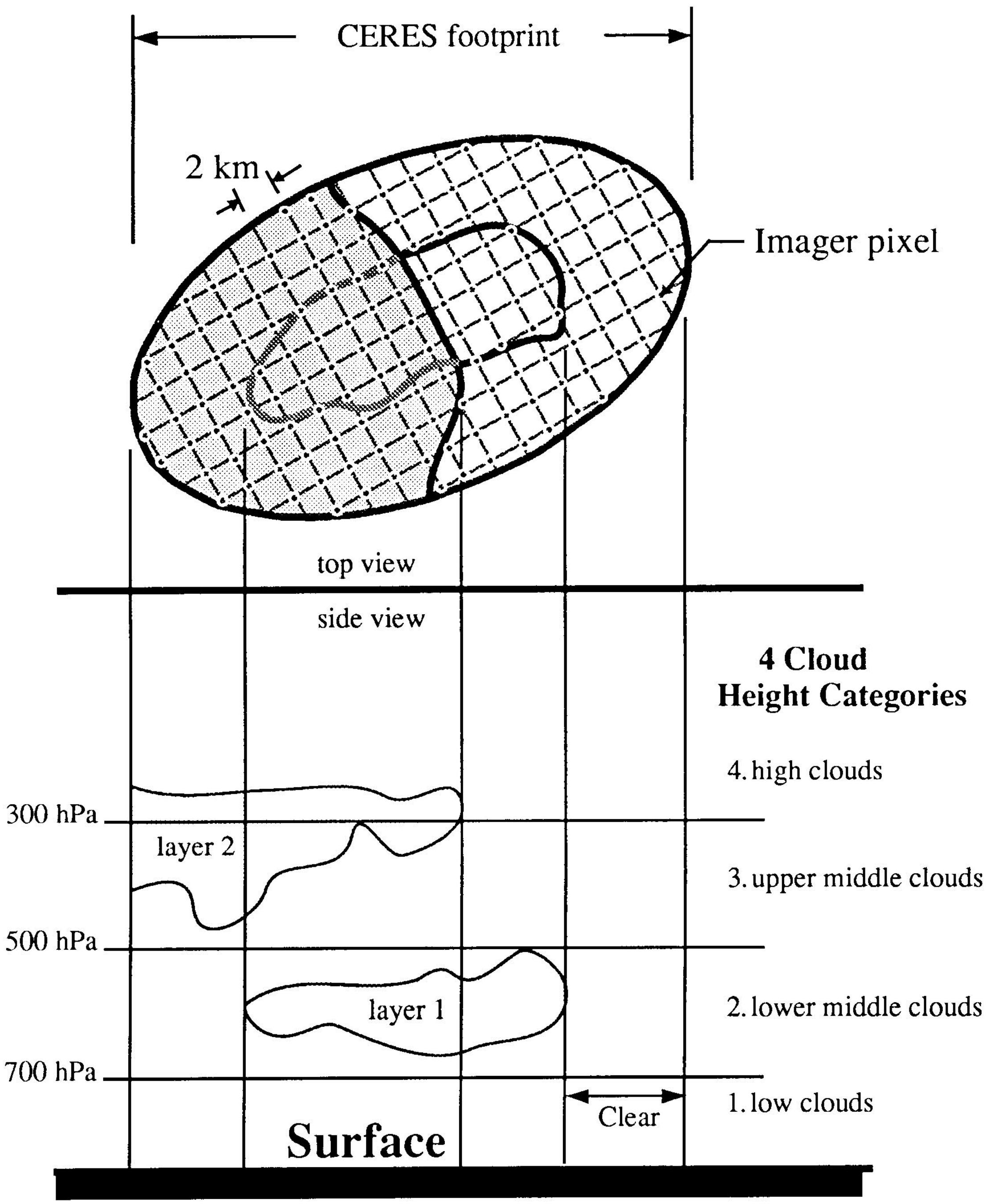

Figure 4.0-4. Schematic diagram of vertical and horizontal cross sections of imager pixel cloud properties matched to CERES field of view. 2-km imager pixel spacing is typical of VIRS on TRMM. Data tables can be found in Subsystem 4.4.

document describes the current understanding of the best way to implement such a combined algorithm. Like ISCCP, the cloud algorithm is divided into a cloud detection and a cloud optical property stage. Unlike ISCCP, the algorithm also includes an additional stage for the determination of well-defined cloud layers. Sections 4.1, 4.2, and 4.3 of this document summarize the current strategy for these three tasks. In each area, multiple algorithms are brought to bear, usually in a hierarchy which depends on either the surface background (ocean, land, mountain, desert, snow/ice) or on the clouds themselves (low, high, thick, thin, single layer, multiple layer). Initially, this combination is likely to cause significant problems. As the CERES team works through the first month of global data in the next year, a better understanding will emerge of our ability to combine the algorithm capabilities.

6. Accurate relationships between cloud and radiative fluxes require accurate spatial and time matching of both imager-derived cloud properties and CERES broadband radiation data.

There are three primary reasons to closely link the instantaneous CERES radiances to cloud imager derived cloud properties.

First, the development of anisotropic models from CERES rotating azimuth plane scanner data requires that CERES broadband radiances be accurately classified as a function of cloud and surface properties. A particularly critical cloud property for SW and LW anisotropy is cloud optical depth. Tests were made using FIRE stratocumulus uplooking passive microwave observations of LWP (e.g., Cahalan et al. 1994) taken every minute for 19 days in July 1987 at San Nicolas Island. At a mean wind speed over the period of 5 m/s, the 1-minute sampling corresponds to a cloud advection of about 300 m. A running time average was then applied to the data to simulate the 20-km CERES footprint scale (roughly a 60-minute running average). Finally, the time-averaged CERES footprint data were time lagged to simulate the effect of a spatial (or temporal) mismatch in the cloud imager data (providing LWP or cloud optical depth) and the broadband radiation data. If the lagged rms difference in LWP is required to be 5% or less, then the 20-km average can be mismatched by no more than 1 km (or about 3 minutes). The rms LWP error was roughly linear in the lag time or distance. We conclude that accurate angular models are likely to require close matching of cloud and radiation data. Further tests will be conducted using Landsat data to extend these 1-D results to two dimensions.

Second, if TOA flux measurements are to be used to constrain the radiative fluxes calculated using cloud imager derived cloud properties, then a close match of these properties must be obtained. Because cloud physical and optical properties are nonlinearly related to radiative fluxes, rms errors in matching cloud and radiation data should be kept to less than 10% to avoid bias errors. Tests of this sensitivity will be conducted using simulations similar to those above, but including radiative flux calculations on high resolution cloud imager properties such as AVHRR Local Area Coverage data.

Third, the complexity of relationships between cloud properties and radiative properties increases as clouds become multilayered. Tian and Curry (1989) found that while single-layer clouds dominated observations at a 45-km scale (similar to a single CERES footprint), multiple-layer clouds dominated at 220 km (similar to an ERBE grid box). This suggests that for some studies, there is an advantage to close ties of cloud properties and radiative fluxes at not only the scale of large grid boxes, but also at the scale of individual CERES footprints.

The CERES strategy is to represent the distribution of energy received at the CERES broadband detectors by the point spread function (Subsystem 4.4). The point spread function includes the effects of detector response, optical field of view, and electronic filters (Subsystem 1). Cloud imager derived cloud properties will be convolved with the CERES point spread function to derive properties appropriately weighted and matched to the CERES fields of view. Note that the nominal 2σ accuracy of the navigation for the EOS and TRMM platforms is less than 1 km, sufficient to allow an accurate mapping of imager pixel data into CERES fields of view.

7. Anisotropy of cloud and surface scenes can be determined by compositing a large ensemble of scenes where each scene is viewed at one instant of time from only 1 or 2 directions.

The rapid variability of clouds in space and time places a fundamental limitation on measuring radiative flux from space. There are no sufficiently homogeneous targets for which a satellite can view all 2π steradians of a “target” at the same time. The flat plate or active cavity instruments which view 2π steradians from satellite altitude respond to about a 2000-km region on the Earth, guaranteeing inhomogeneity. Therefore, all measurements of flux from space require compositing over time. The scanning radiometers such as the Nimbus-7 ERB or ERBE scanners select a small angular field of view in order to measure individual scene types (forest, cumulus, stratus, cirrus, etc.). This requires the conversion of the radiance measured in a single direction to the desired radiative flux. In order to improve spatial sampling over the globe, scanning radiometers usually scan in a cross-track pattern, limiting angle views to a small systematic subset of the full angular space.

For SW radiation, anisotropy is a function of viewing zenith angle, viewing azimuth angle, and solar zenith angle (Suttles et al. 1988; Wielicki and Green, 1989). Typical scanning instruments measure only a small portion of this 3-D angular space. The Nimbus-7 ERB instrument was designed to sacrifice spatial sampling to obtain improved angular sampling over the entire 2π hemisphere (Taylor and Stowe, 1984). ERBE used these observations to develop the 12 ERBE angular distribution models (ADM’s) as a function of cloud fraction and surface type (ocean, land, desert, snow/ice) (Suttles et al. 1988).

Unfortunately, the ERBE models are unsatisfactory for CERES for three reasons. First, postflight analysis (Suttles et al. 1992) has shown that the estimated SW albedo systematically increases with viewing zenith angle and the estimated LW flux decreases with viewing zenith angle. The ERBE models based on Nimbus-7 observations underestimate the amount of anisotropy. Second, the albedo bias is a function of solar zenith angle, and therefore a function of latitude (Suttles et al. 1992), which will affect the inference of equator-to-pole heat transport. Third, the models only depend on cloud amount, so that the rms error in deriving instantaneous fluxes is estimated as roughly 12%. This instantaneous noise is primarily caused by the inability of ERBE and Nimbus 7 to measure cloud optical depth, the largest source of varying anisotropy (Wielicki and Barkstrom, 1991).

Tests of the ADM bias have examined three possible causes: incorrect scene identification by the ERBE maximum likelihood estimation technique (Suttles et, al. 1992; Ye, 1993), incorrect assumptions in building the ERBE ADM’s, and the dependence of ADM’s on spatial scale (Ye, 1993; Payette, 1989). CERES will fly a scanner which will rotate in azimuth angle as it scans in elevation, allowing the development of a new set of ADM’s. All three candidate problems are being examined with current data in preparation for designing the CERES ADM’s.

First, scene identification will be greatly improved by matching VIRS- and MODIS-derived cloud properties to each CERES field of view. This will provide the basic cloud typing for development of new ADM’s. ADM’s will be derived as a function of cloud amount, cloud optical depth/emittance, cloud height, particle phase, and cloud particle size. Second, one of the critical assumptions of the Nimbus-7 and ERBE ADM’s was that cloud anisotropy and cloud albedo are uncorrelated. For the case of increasing cloud optical depth, this is clearly a questionable assumption. This assumption will be removed for CERES by using the radiance pair method discussed in Subsystem 4.5. This method uses the rotating azimuth plane CERES scanner to obtain views of the same target at nearly the same time from two different viewing angles. The pairs are used to obtain reflectance ratios which eliminate the dependence on target albedo. Finally, studies will examine the dependence of field of view spatial scale in testing of new CERES ADM’s.

4.0.4. Algorithm Outline

Because cloud fields are highly variable in space and time, the process of both cloud detection and cloud property determination from space can become very complex. This is true especially over variable backgrounds such as mountains, desert, or snow and ice. As a result, no single cloud algorithm works well for all cloud types over all backgrounds. In order to deal with this complexity, the CERES cloud algorithm has broken this task into three relatively independent functions:

Subsystem 4.1—Imager clear-sky determination and cloud detection.
Subsystem 4.2—Imager cloud height determination.
Subsystem 4.3—Cloud optical property retrieval.

Following the cloud retrieval over a swath of cloud imager data, three final steps are carried out to obtain TOA and surface radiative fluxes for each CERES broadband measurement.

Subsystem 4.4—Convolution of imager cloud properties with CERES footprint point spread function.

Subsystem 4.5—CERES inversion to instantaneous TOA fluxes.

Subsystem 4.6—Empirical estimates of shortwave and longwave surface radiation budget involving CERES measurements.

The final result is a set of cloud properties and radiative fluxes for each CERES footprint. The final cloud properties are grouped into four cloud height categories with height boundaries at pressures of 700, 500, and 300 hPa. Since more than one cloud layer is allowed in a CERES footprint, we also save the fraction of the footprint covered by cloud imager pixels which showed evidence of overlap of any two of the four cloud height categories. Only two of the four cloud height categories are allowed to overlap in a single cloud imager pixel. For Release 1, we assume that the four cloud height categories are independent, so that cloud properties in any given height category are independent of whether or not they were overlapped with any other height category. This simplification allows us to keep cloud properties for only four categories, as opposed to all possible combinations of cloud height categories. Cloud overlap is only saved as the fractional area of overlap between all combinations of two of the four cloud height categories. Note that while ISCCP saved frequency distributions of a bispectral histogram of cloud optical depth classes and cloud height classes, this leads to a substantial discretization error in determination of average cloud height within a height class. CERES saves not only the frequency of occurrence, but also the average and standard deviation of all cloud properties separately for each cloud height category. In this case, even very small cloud height shifts can be detected within each cloud height category.

All cloud properties are weighted with the CERES point spread function so that CERES-measured broadband TOA fluxes can be used to directly constrain radiative calculations of surface and in-atmosphere fluxes produced using the cloud imager cloud properties. These CERES footprint averages represent a very specific view or composite of cloud physical and optical properties designed to facilitate studies of the role of clouds in the Earth's radiation budget. A table of the CERES cloud products for each CERES footprint can be found in Subsystem 4.4.

Finally, where possible, direct parameterizations of TOA radiative fluxes to surface radiative fluxes are derived. These surface flux estimates for each CERES footprint are saved in the SSF output product of Subsystem 4, as well as in spatially gridded and time-averaged forms in the SURFACE products (Subsystems 9 and 10). Direct parameterization of TOA to surface fluxes is used as an alternative approach to the calculation of surface radiative fluxes using cloud properties and radiative models used in the ATMOSPHERE data products (Subsystems 6, 7, and 8).

A full description of the Subsystem 4 input and output products can be found in appendixes A and B.

4.0.5. Algorithm Releases

The CERES algorithm will be designed in four phases or "releases." Version 0 is an experimental version to test initial concepts in an informal way. Version 0 was a layer bispectral threshold method (Minnis et al. 1993) which determined cloud fraction in three vertical layers. It is similar to the ISCCP technique in that fixed differentials are added to the expected clear-sky visible (0.65 μm) and infrared (10.8 μm) radiances to set thresholds for cloud detection. Data from the 3.7-μm channel are used to detect snow. Optical depth is calculated (section 4.3.4.1.1) using the visible channel and one of two microphysical models: 10-μm water spheres for cloud temperatures warmer than 253K, and cirrostratus hexagonal ice crystals (Takano and Liou, 1989) for colder clouds. Visible optical depth is converted to 10.8-μm absorption optical depth and then used to correct cloud altitudes for emittances less than 1 (section 4.3.4.4). The version 0 code was applied to NOAA-9 October 1986 AVHRR and ERBE data. The AVHRR global area coverage (GAC) pixels were matched to ERBE footprints using an 8×8 array of GAC data centered on the ERBE footprint. The analysis incorporated many of the same inputs that will be used in the later CERES cloud algorithm versions. Analysis results were provided for use in initial testing of the calculation of in-atmosphere fluxes in Subsystem 5.

Release 1 will be operational by 1995, and is designed to process global data from the existing NOAA-9 and NOAA-10 ERBE/AVHRR/HIRS data. This release will be used to test algorithm concepts on global data, and for comparing multiple algorithms for cloud parameters such as cloud height. This is a critical step, since most of the algorithms have only been used for specific regional studies. This step will expose much of the exception handling required to run a global analysis. In addition, many of the sensitivity studies needed to test time interpolation/averaging algorithms in Subsystems 7, 8, and 10 require geostationary data analyzed at hourly intervals. Data from GOES-8, launched in the Spring of 1994, will provide the opportunity to test the CERES Release 1 algorithms on geostationary data very similar in spatial resolution and spectral channels to the AVHRR/HIRS combination on NOAA 9 and 10.

Release 2 will be ready by early 1997, in time to integrate into the Langley DAAC (Distributed Active Archive Center) before the TRMM launch of the first CERES instrument planned for August, 1997. Release 2 will be designed to operate on TRMM data, including the CERES broadband scanner data and the VIRS cloud imager data. Release 2 will also incorporate the use of the TMI (TRMM Microwave Imager) LWP measurements for multilayer clouds over ocean. This release will not use any infrared sounder channel analysis (these channels are missing from VIRS) but will incorporate the VIRS 1.6-μm channel for improved particle size determination. In addition, this release may use the VIRS 0.65- and 1.6-μm channels to obtain estimates of aerosol optical depth based on the NOAA AVHRR operational algorithm. The advanced NOAA aerosol algorithm using the 0.65- and 1.6-μm channels of AVHRR should have been tested for 2 years prior to the TRMM launch.

Release 3 will be designed to use the MODIS cloud imager data, as well as the CERES rotating azimuth plane scanner which will be used to develop new empirical models of the anisotropy of SW and LW radiances. This release will be used to process EOS-AM and EOS-PM data. Until new angular models are developed, the CERES analysis will rely on the ERBE models (Suttles et al. 1988) to convert the measured broadband radiance to a TOA broadband flux. Note that the MIMR (Multifrequency Imaging Microwave Radiometer) passive microwave instrument will be available on the EOS-PM platform and on an ESA (European Space Agency) polar-orbiting platform in the same orbit at EOS-AM. These MIMR instruments will provide the estimates of cloud liquid water path.

4.0.6. Validation

The CERES investigation directly funds CERES science team members and support staff to carry out validation investigations. These investigations typically involve tests of various algorithm components (cloud height, particle size, etc.) against field experiment data such as that obtained by the FIRE and ARM projects.

Current data used for *simulation* of CERES cloud and flux inversion algorithm capabilities include

Satellite data:

- AVHRR/HIRS to simulate most of the VIRS and MODIS channels
- Landsat to simulate the higher spatial resolution of MODIS, as well as measurements of 1.6 and 2.1-μm channels not on AVHRR or HIRS.
- GOES radiance and ISCCP cloud data to test time sampling of cloud properties
- Nimbus-7 ERB and ERBE broadband data to test angular modeling
- GOES-8 (similar to AVHRR/HIRS channels)

Aircraft data:

- MAS on the ER-2 in FIRE, ARM, SCAR (Sulfates, Clouds, and Radiation), etc.
- Thematic Mapper Simulator on the ER-2

Current data used to *validate* the satellite cloud and flux inversion algorithms include

- ER-2 lidar collocated with Landsat, AVHRR, HIRS, and MAS data (cloud top)
- Surface-based lidar (cloud base, tops for thin clouds)
- Surface-based 3-mm and 8-mm radar (cloud base and top)
- Surface- and ER-2-based passive microwave for LWP (cloud LWP)
- Landsat and ER-2 data for cloud detection accuracy (cloud area)
- Aircraft microphysical probes (cloud particle size, phase, habit)
- Multi-instrument comparisons: AVHRR vs. HIRS cloud height for thin cirrus
- ER-2 CCD (charged coupled device) array imager to examine cloud anisotropy at solar wavelengths
- CAR (Cloud Absorption Radiometer) to examine cloud single scattering albedo, and angular reflectance patterns (scans from nadir to zenith, 0.5 to 2.5 m channels)
- LITE on space shuttle for 5 days in September 1994: First global measurement of lidar cloud height; space scales and AVHRR underflights

Future data sets used to *validate* satellite cloud and flux inversion algorithms include

- NOAA U.S. ceilometer network (cloud base to 4-km altitude)
- LITE (future missions)
- ADEOS (Advanced Earth Observing System; ESA, Japan 1996 a.m. sun-synchronous) POLDER (Polarization and Directionality of Earth's Reflectances) instrument for polarization and multiangle CCD array measurements at solar wavelengths
- EOS-AM platform (1998) ASTER (Advanced Spaceborne Thermal Emission and Reflection Radiometer) instrument (Landsat-like spatial resolution, but adds thermal channels at 3.7, 8.5, 11, and 12 m similar to MODIS)
- EOS-AM platform MISR (Multiangle Imaging Spectroradiometer) multiangle CCD array cameras for SW anisotropy at spatial scales from 200 m to 300 km, and stereo cloud height
- EOS-PM platform (2000) MIMR passive microwave instrument [improved Special Sensor Microwave/Imager (SSM/I) for LWP]
- EOS GLAS (Geoscience Laser Altimeter System; 2002) a nadir pointing space-based lidar for validation of global cloud height observations
- Space-based 3 mm radar (under discussion but not scheduled for flight: Cloud top and cloud base, plus multilevel cloud validation)
- Field experiment data including

    FIRE: Expected to examine polar boundary layer cloud and tropical cirrus (1997, 1998). Includes in-cloud and surface radiative flux data

    CEPEX (Central Equatorial Pacific Experiment) and TOGA-COARE (Tropical Ocean Global Atmosphere Coupled Ocean-Atmosphere Response Experiment): 1992/1993 tropical cloud experiments

    GCIP [GEWEX (Global Energy and Water Cycle Experiment) Continental-Phase International Project]: Expected to examine continental U.S. clouds; Mississippi basin (1996 and later). Primarily ceilometers and surface radiative fluxes

    ARM: Oklahoma, western Pacific Ocean, and Alaskan north slope surface sites. These sites include surface radiation, lidar, cloud radar, and profilers. Data available over next few years and extending over a 10-year period

    SHEBA (Surface Heat and Energy Balance of the Arctic): A surface site on the polar ice cap for 18 months (1997). Includes lidar and surface radiation budget data

WBSRN (World Baseline Surface Radiation Network): Surface radiative fluxes

Other field experiments of opportunity: BOREAS (Boreal Ecosystem Atmosphere Study), SCAR, etc.

CERES science team members are active members of many of the field experiment programs including FIRE, ARM, GCIP, WBSRN, CEPEX, TOGA-COARE, and SCAR programs. These relationships, along with CERES investigator funding will be used to develop and carry out validation plans for specific components of the CERES cloud and radiative flux inversion algorithms discussed in Subsystems 4.1–4.6. CERES does not, however, have funding to carry out its own field experiments. CERES is dependent on these other programs for validation data. Many of the results shown in the subsystem ATBDs and used to plan the current CERES algorithms are a result of CERES science team participation in these programs to date.

4.0.7. Processing Estimates

Processing resources required have been estimated by scaling existing satellite analysis codes including the ERBE inversion subsystem (Wielicki and Green, 1989) processing global ERBE data, the Spatial Coherence cloud algorithm running on 4-km AVHRR data, the HBTM (Hybrid Bispectral Threshold Method) running on 4-km AVHRR data (Minnis et al. 1993), a two-channel ISCCP-like (CERES version 0) algorithm running on 4-km AVHRR data, and finally a newly developed research code incorporating more of the CERES algorithms, but without optimization (see Subsystem 4.3).

In order to estimate the requirements for VIRS and MODIS processing, these processing times were scaled linearly by

- Number of imager pixels to be processed
- Number of imager spectral bands to be processed
- An increased total algorithm complexity of a factor of 4 times the ERBE, spatial coherence, and ISCCP-like V0 algorithms, and a factor of 2 times the new research algorithm
- A requirement for the algorithm to run three times faster than real time (i.e., 3 days of global data for one instrument processed in 1 day)

All algorithms were run on Sun Sparc 2 systems with an assumed floating point computational power of 4.0 million floating point operations per second.

We scaled the timings to process five spectral bands on VIRS (2-km spatial resolution), and to process 11 spectral bands on MODIS, including two 250-m spatial resolution spectral bands (day only), two 500-m bands (day only), and seven 1-km bands (day and night). The timing estimates in Gflops (billions of floating point operations per second) were:

	ERBE	ISCCP V0	Spatial Coherence	New Research Algorithm
VIRS:	0.5	0.7	0.7	4.5
MODIS:	7.5	12.2	12.2	78.

The highest processing loads were from a new unoptimized research code, and should reduce by a factor of 2–10 with optimization. Overall, estimates appear to be about 0.7 Gflop for VIRS and 10 Gflops for MODIS full resolution data. We will examine the accuracy degradation in subsampling the MODIS data to 1/4 of the MODIS pixels. This accuracy issue is primarily for matching instantaneous cloud property data to CERES fields of view for the radiative flux calculations performed in Subsystem 5. If cloud properties include too high a spatial sampling noise, then constraints against TOA measured fluxes are more difficult and less accurate. This subsampling issue will be examined using 1-km AVHRR data and simulating the CERES point spread function.

For large data volumes, there is a common conception that processing is I/O (input/output) bound, even for hard disk I/O. To test this, we examined the time to perform the following processes on a 10-Mbyte Landsat data file:

10 seconds = Read data from hard disk (SCSI-1 on a Sun Sparc 2) to memory
43 seconds = Unpack the data from scan line records to pixel byte data (16-bit digital count) using an optimized routine for unpacking data
24 seconds = Convert the digital count data to real radiance values (32 bit) using a simple look-up table

We found that for even this simple process, that only 13% of the total time was spent in reading the data, while the processing burden of unpacking and calibrating dominated the processing time. For a complete cloud algorithm which then analyzes the radiance data, the I/O fraction will be 1% or less. This trade-off will be examined further with much higher power processors such as an SGI machine using a 4400 processor at greater than 30 million floating point operations per second. The critical I/O issue is more likely to occur in reading the archive media.

Given the rapid improvement in microprocessor speeds, it is likely that super workstations will be capable of processing the VIRS and later MODIS data streams. The larger problem may well be data storage. For the MODIS and VIRS data, the Langley DAAC will not keep a separate level 1b archive, but will only keep data for the last month or two to simplify data storage. Any later reprocessing would return to the GSFC DAAC to obtain the required MODIS level 1b data.

4.0.8. Relationship of MODIS and CERES Cloud Data Products

4.0.8.1. Background. One of the comments of the peer review panel was that CERES and MODIS Science Teams are both producing estimates of cloud properties. Is this a duplication of effort? Can't one cloud product satisfy all users?

If we view clouds as large (relative to satellite image pixels), well-defined, and well-behaved sheets of paper floating in the atmosphere, then one cloud definition will suffice for all users. We simply define whether the sheet is present or not, the altitude of cloud occurrence, and the properties of the cloud sheet.

Field experiments show that actual clouds

- Change on time scales of seconds to hours (much less than satellite revisit time)
- Change on space scales from meters to 10 000 km (much less than to much greater than satellite pixel size)
- Have highly variable shapes and configurations
- Occur at least half the time in multiple overlapping cloud layers
- Often have optically thin cloud edges; no sharp cloud/clear boundary (boundary layer clouds)
- Are often sufficiently optically thin to be at the edge of detectability with passive radiometers (cirrus clouds)

Given this extreme variability, and the associated difficulty in accurately remotely sensing cloud properties, it is unlikely that a single approach to cloud measurement will meet all needs.

4.0.8.2. EOS cloud products. In particular there are three major categories of cloud data required: cloud masking, cloud physical properties, and cloud radiative properties. For each of these areas, the MODIS and CERES teams are cooperatively examining a range of strategies to derive cloud properties. A comparison of MODIS and CERES cloud products is given in Table 4.0-1. The table gives the primary *focus* of each product, *not* its only use. The focus, or top priority, however, controls the future processing strategies and adjustments as we learn more about clouds using the EOS and field experiment observations.

Table 4.0-1. Comparison of MODIS and CERES Cloud Products

MODIS: Daytime solar channels (King)	MODIS: Day/night infrared HIRS-like clouds (Menzel)	CERES: Day/night, solar/lnfrared VIRS-like clouds (Barkstrom)
Cloud dynamics	Cloud dynamics	Cloud radiative effects
Daytime only	Daytime and nighttime	Daytime and nighttime
Instantaneous	Time averaged	Time averaged
Pixel to global scale	Regional to global scale	Regional to global scale
Rapid algorithm improvement	Infrequent algorithm improvement	Slow algorithm improvement
Time series inconsistency allowed	Time series must be consistent	Time series must be consistent
Algorithm change MIGHT = Reprocessing	Algorithm change MUST = Reprocessing	Algorithm change MUST = Reprocessing
Subset of cloud properties OK *(all retrieved properties high accuracy)*	Subset of cloud properties OK *(all retrieved properties high accuracy)*	Complete cloud properties required *(some cloud properties low accuracy such as cloud thickness and base)*
Cloud properties stand alone	Cloud properties must be consistent with existing HIRS data	MODIS/VIRS must be consistent *(at least in early years of EOS)*
Avoid marginal cloudy/clear data in time and space averaged data	Include marginal cloudy/clear data in time and space averaged data	Include marginal cloudy/clear data in time and space averaged data

1. ***Cloud masking: Determination of each satellite pixel as either cloud-free or cloud contaminated.***

Masking determines if a satellite pixel is a candidate for use in observing surface properties after correction for atmospheric effects. For example

- SST (sea surface temperature) observations: optically thin boundary layer cloud is acceptable (small thermal infrared impact) while optically thin cirrus is damaging (relatively large thermal infrared effect). Cloud shadows have no effect.
- Vegetation canopy studies: More thin cirrus is allowable, but need to avoid cloud shadows.
- Fields of view which are uncertain (could be clouds or clear) will usually be ignored in MODIS time and space averages of cloud and surface properties. These data will be included in the CERES time and space averages of cloud properties for radiation budget purposes.

2. ***Cloud physical properties: Cloud property estimates for use in characterizing cloud properties over the globe, and for testing dynamical models of clouds.***

Emphasis is on getting accurate cloud water budget: liquid water, ice water, cloud amount, height, and particle size/phase. Statistics in a grid cell, or over a type of cloud, are most critical, since a simulated cloud field can never be expected to match real clouds cell for cell (predictability problem and inadequate model initialization at cloud scale). Primary emphasis is on provision of regional cloud properties with highest accuracy, but availability depends on actual cloud conditions. Secondary emphasis is on global scale properties. As improvements in cloud remote sensing are developed using MODIS, they are implemented, with improvements every 3–6 months shortly after launch and at 1–2 year intervals thereafter. Reprocessing of the previous data is decided on a case by case basis. Accuracy of current data is more important than a single consistent time record.

Cloud properties vary greatly in their effect on solar radiation (scattering dominated) as opposed to thermal infrared radiation (absorption and emission dominated). MODIS will exploit this difference to pursue two different strategies for determining cloud physical properties. One set of cloud data (King; see Table 4.0-1) will focus on information retrieved using solar reflectance channels on MODIS to derive cloud particle size and cloud optical depth during daytime observations. A second set of cloud data (Menzel; see Table 4.0-1) will focus on information retrieved using the thermal infrared channels on MODIS to derive cloud effective emittance, cloud height, and cloud particle size. Each technique has advantages and disadvantages that will be useful in studies of clouds. The thermal infrared cloud data will also extend in time a global cloud data set started using the NOAA HIRS/2 data. For climate record analysis, the infrared cloud analysis technique will be consistent for the HIRS and MODIS data sets.

3. ***Cloud radiative properties: Cloud property estimates for use in determining the radiation budget at the top of the atmosphere, within the atmosphere, and at the surface, and for studying the role of clouds and radiation in the climate system.***

Many studies of cloud/climate feedback mechanisms will require cloud and radiation budget data which are internally consistent. For CERES (Barkstrom; see Table 4.0-1), the emphasis is on radiatively effective cloud data. Emphasis is also on global data available at all times and places. Secondary emphasis is on regional studies. Because climate data must be stable for long periods of time, algorithms are updated very infrequently, perhaps once every 3–5 years. When algorithms are updated, all previous data are reprocessed with the new algorithms. A single consistent time record is of primary importance; accuracy of current data is of secondary importance. As an example, CERES will have flown on the TRMM spacecraft 1 year before the launch of EOS-AM. Accurate determination of the diurnal cycle of radiation will require combination of TRMM, EOS-AM, and EOS-PM data. But the TRMM cloud imager (VIRS) is not as capable as the MODIS instrument on EOS-AM and EOS-PM. VIRS has a larger footprint, and has only half of the MODIS channels useful for cloud property analysis. CERES will need to maximize the consistency between VIRS and MODIS cloud properties, thereby maximizing the time sampling information provided by the TRMM precessing orbit. A trade-off will result; the CERES analysis of MODIS data will strive for consistency with VIRS on the one hand, and full utilization of MODIS on the other. The trade-off will be decided by examining the impact of the decision on derived CERES radiative fluxes. The likely result is that CERES will sacrifice some of the MODIS cloud property accuracy for consistency with TRMM cloud data from VIRS. The MODIS team, in contrast, will seek to utilize the full capability of the MODIS data for cloud physical properties.

4.0.8.3. Data processing cost issues. At a recent workshop on the future projections for computing capabilities in the late 1990’s (Skamania, October 1994), two conclusions were reached:

- Flops and baud will be free [i.e., processing power and data transfer rates (bits per second for sequential data transfer) will get very cheap].
- Data storage costs will not fall nearly as fast. Data random access times will also fall much slower.

The conclusion is that the additional cost of processing data twice in a global streaming mode (process all data in time-ordered fashion) will be inexpensive. The cost to send the full MODIS level 1b data stream (about 20 Mbps) to LaRC in 1998 is estimated to be less than $10K per year in line charges, and would require about 1/7 the bandwidth of a common 155 Mbps ATM (asynchronous transfer mode) data line in 1998. Further, since CERES is processing climate data, there is no need for immediate MODIS processing. Up to a 1-month delay is acceptable. In this case, even if ATM data line availability is delayed beyond 1998, the MODIS data could be copied to high density tape and transported between the GSFC and Langley DAAC’s until the ATM lines are available. There is also no need to archive the MODIS level 1b data at Langley. LaRC would keep the last 2 months of data on a revolving archive for current processing. Over 5 years of MODIS data, this archive cost is 3% of the total MODIS archive at GSFC. Reprocessing the CERES data is seldom done (say every 5 years) so that frequent access to

MODIS data is not required by the operational CERES processing. When MODIS level 1b data are required for reprocessing of CERES data, reprocessing is efficiently done in a streaming mode with the newest, perhaps recalibrated, MODIS level 1b data retransmitted from the GSFC archive.

4.0.8.4. Summary. The role of clouds and radiation in the climate system is the highest priority science issue in the U.S. Global Change Research Program. Solutions to this problem will be very difficult, and therefore should be approached from distinctly different perspectives to maintain program robustness. The cost of processing two different views (dynamical and radiative) of cloud properties using the MODIS data is a very small fraction of the cost of building, flying, and operating the MODIS instrument and processing the data.

Any single cloud algorithm team will be subject to a “one size fits all” approach. This approach will not be optimal for any cloud data use and will suppress new creative solutions to problems. On the other hand, the current uncertainties are sufficiently large that in a room of 12 cloud researchers one is likely to find 12 different proposed cloud algorithms. EOS cannot afford to support all possibilities, but must, however, support a few key strategies best suited to the EOS observational capabilities.

We propose that CERES provide a cloud data set focused on the needs of the cloud radiation budget science issues and that MODIS provide a data set focused on the needs of cloud dynamics and cloud processes science issues.

Note that MODIS and CERES are not the only investigations which will provide critical contributions needed for cloud/climate research. In particular

- MISR will provide unique simultaneous multiangle solar reflectance observations to verify the radiative modeling of inhomogeneous cloud cells and cloud fields. MISR will also provide independent verification of cloud heights using stereo viewing techniques.
- AIRS (Atmospheric Infrared Sounder) will provide unique high spectral resolution infrared observations of clouds that will allow more complete examination of cloud microphysics at night, and a consistent day/night subset of cloud properties.
- ASTER will provide very high spatial resolution data (15–90 m) for verification of the effects of beam filling on global data derived using coarser resolution sensors such as MODIS and VIRS.
- EOSP (Earth Observing Scanning Polarimeter) polarization measurements offer the best hope of distinguishing ice particle shape.
- Eventually, cloud lidar (thin clouds) and cloud radar (thick clouds) will be required to verify the EOS capabilities for overlapped multilevel cloud conditions.

MODIS and CERES provide the two most comprehensive global cloud data sets for global change studies. But there are additional critical contributions made by other instruments that also will be necessary to solve the role of clouds in the climate system.

Appendix A

Input Data Products

Determine Cloud Properties, TOA and Surface Fluxes (Subsystem 4.0)

This appendix describes the data products which are used by the algorithms in this subsystem. Table A-1 below summarizes these products, listing the CERES and EOSDIS product codes or abbreviations, a short product name, the product type, the production frequency, and volume estimates for each individual product as well as a complete data month of production. The product types are defined as follows:

Archival products:	Assumed to be permanently stored by EOSDIS
Internal products:	Temporary storage by EOSDIS (days to years)
Ancillary products:	Non-CERES data needed to interpret measurements

The following pages describe each product. An introductory page provides an overall description of the product and specifies the temporal and spatial coverage. The table which follows the introductory page briefly describes every parameter which is contained in the product. Each product may be thought of as metadata followed by data records. The metadata (or header data) is not well-defined yet and is included mainly as a placeholder. The description of parameters which are present in each data record includes parameter number (a unique number for each distinct parameter), units, dynamic range, the number of elements per record, an estimate of the number of bits required to represent each parameter, and an element number (a unique number for each instance of every parameter). A summary at the bottom of each table shows the current estimated sizes of metadata, each data record, and the total data product. A more detailed description of each data product will be contained in a User's Guide to be published before the first CERES launch.

Table A1. Input Products Summary

Product Code						
CERES	EOSDIS	Name	Type	Frequency	Size, MB	Monthly Size, MB
CID_MODIS	CERX04	MODIS Cloud Imager Data	Ancillary	1/Hour	2491.0	1853304
CID_VIRS	CERX05	VIRS Cloud Imager Data	Ancillary	1/Hour	71.1	52898
CRH	CER16	Clear Reflectance History	Archival	Every 10 Days	91.1	282
IES	CER09	Instrument Earth Scans	Internal	1/Hour	16.7	12425
MOA	CERX06	Meteorological, Ozone and Aerosols	Archival	1/Hour	10.5	7797
MWP	CERX08	Microwave Liquid Water Path	Ancillary	1/Day	25.0	775
SURFMAP	CERX07	Surface Map	Ancillary	1/Week	82.8	367

MODIS Cloud Imager Data (CID_MODIS)

The MODIS cloud imager data (CID_MODIS) from the EOS spacecraft is level 1b data from 11 of the MODIS channels. The data coverage is 1 hour. The product has a header record followed by multiple scan line records. The organizational details of this product are not finalized yet. Each pixel in the scan line record has radiance values for each of the channels. In addition, each scan line record contains time, location, and solar angle data. It is assumed that the data are organized in the scan lines that appear to scan in the same direction for each scan.

The channels requested by the CERES Science Team are

Channels	Wavelength, µm	Resolution (km)
Channel 1	0.645	0.25
Channel 6	1.64	0.50
Channel 7	2.13	0.50
Channel 20	3.75	1.0
Channel 26	1.375	1.0
Channel 29	8.55	1.0
Channel 31	11.03	1.0
Channel 32	12.02	1.0
Channel 33	13.335	1.0
Channel 34	13.635	1.0
Channel 35	13.935	1.0

The CERES Science Team has requested averaged data from the 1/4-km resolution channel to 1/2 km and 1 km, and the two 1/2-km resolution channels averaged to 1-km resolution. The cloud sytem thus requires input data from the 11 channels and the 4 averaged data sets for a total of 15 sets of “channel” data.

The CID_MODIS product is external to the CERES processing and is released after CERES processing is completed. It is assumed that the responsible EOSDIS DAAC would retain a copy of this product should it be needed by CERES for a rerun.

Level: 1b
Type: Ancillary
Frequency: 1/Hour

Time Interval Covered
File: 1 Hour
Record: 1 MODIS Scan

Portion of Globe Covered
File: Satellite Swath
Record: 1 Scan

Portion of Atmosphere Covered
File: Satellite Altitude

Table A2. MODIS Cloud Imager Data (CID_MODIS)

Description	Parameter Number	Units	Range	Elements/ Record	Bits/ Elem	Elem Num
CID_MODIS						
MODIS header record		N/A	N/A	1	2048	
MODIS_Record is Array[25000] of:						
MODIS_Scanline						
MODIS_Pixels is Array[52240] of:						
MODIS channel and FOV data	1	N/A	TBD	52240	16	1

Total Meta Bits/File:	2048
Total Data Bits/Record:	835840
Total Records/File:	25000
Total Data Bits/File:	20,896,000,000
Total Bits/File :	20,896,002,048

VIRS Cloud Imager Data (CID_VIRS)

The VIRS cloud imager data (CID_VIRS) is received from the VIRS instrument on the TRMM spacecraft. We are requesting level 1b data from the five VIRS channels. The data coverage is 1 hour. The product has a header record followed by multiple scan line records. Each scan line has

Pixel location
Spacecraft position
Channel data
VIRS pixel data
Solar viewing angles

Each pixel in the scan line record has radiance values for each of the channels. It is assumed that the data are organized in scan lines that appear to scan in the same direction for each scan.

The CID_VIRS product is external to the CERES processing and is released after CERES processing is completed. It is assumed that the responsible EOSDIS DAAC would retain a copy of this product should it be needed by CERES for a rerun.

Level: 1b
Type: Ancillary
Frequency: 1/Hour

Portion of Globe Covered
File: Satellite Swath
Record: 1 Scanline

Time Interval Covered
File: 1 Hour
Record: 1 Scan each 3.4 sec

Portion of Atmosphere Covered
File: Satellite Altitude

Table A3. VIRS Cloud Imager Data (CID_VIRS)

Description	Parameter Number	Units	Range	Elements/ Record	Bits/ Elem	Elem Num
CID_VIRS						
VIRS_Header						
Julian date of product start day		day	TBD	1	32	
Fractional Julian time of product start time		day	0.0 - .999999999	1	32	
Name of spacecraft carrying imager instrument		N/A	N/A	1	32	
Observing imager name		N/A	N/A	1	32	
Number of imager channels considered		N/A	1 .. 5	1	16	
Number of scan lines		N/A	0 .. 11,808	1	32	
VIRS_Scanline is Array[11808] of:						
VIRS_Scan_Line_Definition						
Year, day, hour, minute, second time code	1	count	TBD	1	48	1
Angular velocity	2	rad sec^{-1}	TBD	1	32	2
Location is Array[261] of:						
Pixel_Location						
Latitude of imager pixel	3	deg	-90 .. 90	261	32	3
Longitude of imager pixel	4	deg	-90 .. 90	261	32	264
Scan angle of imager pixel	5	deg	TBD	261	16	525
Spacecraft_Dynamic_Parameters is Array[3] of:						
Spacecraft_Position						
xdot, ydot, zdot	6	m sec^{-1}	TBD	3	32	786
pitch, roll, yaw	7	deg	TBD	3	32	789
x, y, z position	8	m	TBD	3	32	792
Additional_Requirements						
Scan number	9	N/A	0 .. 11,808	1	16	795
Quality flag	10	N/A	TBD	1	32	796
Number of meaningful viewing angles appended to scan	11	N/A	TBD	1	8	797
Angles_VIRS is Array[261] of:						
Angles						
Solar zenith angles from imager	12	deg	0 .. 90	261	8	798
Viewing zenith angles from imager	13	deg	0 .. 90	261	16	1059
Viewing azimuth angles from imager	14	deg	0 .. 180	261	8	1320

Table A3. Concluded

Description	Parameter Number	Units	Range	Elements/ Record	Bits/ Elem	Elem Num
VIRS_Pixels is Array[261] of:						
Channel_Data						
Channel 1, .63 micrometers (visible), day only	15	$W\text{-}m^{-2}sr^{-1}\mu m^{-1}$	TBD	261	16	1581
Channel 2, 1.6 micrometers (near infrared), day only	16	$W\text{-}m^{-2}sr^{-1}\mu m^{-1}$	TBD	261	16	1842
Channel 3, 3.75 micrometers (infrared), day and night	17	$W\text{-}m^{-2}sr^{-1}\mu m^{-1}$	TBD	261	16	2103
Channel 4, 10.7 micrometers (infrared, clouds), day and night	18	$W\text{-}m^{-2}sr^{-1}\mu m^{-1}$	TBD	261	16	2364
Channel 5, 12.0 micrometers (infrared, moisture), day and night	19	$W\text{-}m^{-2}sr^{-1}\mu m^{-1}$	TBD	261	16	2625

Total Meta Bits/File:	176
Total Data Bits/Record:	50536
Total Records/File:	11808
Total Data Bits/File:	596729088
Total Bits/File :	596729264

Clear Reflectance History (CRH)

The clear reflectance/temperature history (CRH) data are organized on a global equal-area grid that is approximately 10 km by 10 km. The data coverage is 24 hours, and is updated every 10 days from the clear reflectance/temperature history database (CRH_DB). The CRH_DB has the same structure as CRH, and is updated twice a day if clear-sky conditions exist for the particular grid cell. The data product consists of a product header followed by fixed-length records organized according to the grid pattern. Each record has

Visible albedo
Temperature
Viewing angles

The parameters are derived from cloud imager measurements by Subsystem 4. The CRH product is the same structure for both MODIS values and VIRS values. There is a source indication on the header record. The CRH is archived so that the CERES investigation will have access to any particular day throughout the life of the mission, and it is needed for reprocessing.

Level: 3
Type: Archival
Frequency: Every 10 Days

Time Interval Covered
File: Life of Mission
Record: Every 10 Days

Portion of Globe Covered
File: Entire Globe
Record: 10km by 10km grid

Portion of Atmosphere Covered
File: Surface Reference

Table A4. Clear Reflectance History (CRH)

Description	Parameter Number	Units	Range	Elements/ Record	Bits/ Elem	Elem Num
CRH						
CRH header record		N/A	N/A	1	2048	
Record_CRH is Array[4341600] of:						
Grid_CRH						
Day of observation	1	day	Mission Life	1	32	1
Time of observation	2	day	0..1	1	32	2
Visible albedo for collimated, overhead sun illumination	3	N/A	0 .. 1	1	16	3
Temperature derived from 3.7 µm imager channel	4	K	TBD	1	16	4
Temperature derived from 11 µm imager channel	5	K	TBD	1	16	5
Solar zenith angle from imager	6	deg	0 .. 90	1	16	6

Table A4. Concluded

Description	Parameter Number	Units	Range	Elements/ Record	Bits/ Elem	Elem Num
Mean imager viewing zenith over CERES FOV	7	deg	0 .. 90	1	16	7
Mean imager relative aziumth angle over CERES FOV	8	deg	0 .. 360	1	16	8
Narrowband ADM Type	9	N/A	TBD	1	16	9

Total Meta Bits/File:	2048
Total Data Bits/Record:	176
Total Records/File:	4341600
Total Data Bits/File:	764121600
Total Bits/File :	764123648

Instrument Earth Scans (IES)

The IES data product contains the equivalent of 1 hour of data from a single CERES scanner. The data records are ordered along the orbital ground track, with each footprint position related to the spacecraft's suborbital point at the start of the hour. The spatial ordering of records within this product will ease the comparison of CERES data with cloud imager data in subsystem 4. The footprint record is the basic data structure for this data product. This record contains the following kinds of information:

1. Time of observation
2. Geolocation data (at both the top of atmosphere (TOA) and at Earth's surface)
3. Filtered radiances (at satellite altitude), with associated quality measures
4. Spacecraft orbital data
5. Footprint viewing geometric data

The IES data product contains only measurements that view the Earth. For the TRMM mission, this means that approximately 225 Earth-viewing footprints (records) are stored on the IES from each 3.3-second half-scan. Because the Earth scan pattern of the CERES instrument in the biaxial scan mode is irregular, the exact number of pixels in each IES data product varies. This variation is caused by the lack of predictability of the azimuth position at both the start and end of the hour. If the azimuth angle near the start (or end) of an hour is near the crosstrack position, then the number of footprints in the IES product is near the estimated value given below. If the azimuth angle is near the alongtrack position, some of the footprints are instead spatially located within the previous (or next) hours IES. Thus, we have used an estimate of the number of 3.3-second half-scans per hour (approximately 1091) times the number of Earth-viewing measurements in a half-scan (TRMM estimate is 225, EOS estimate is 195) to arrive at our IES product sizing. For TRMM, this is estimated as 245 475 measurements per IES data product and for EOS the estimate is 212 745 measurements. The larger of these two measures is used to determine product sizing.

Level: 1b
Type: Internal
Frequency: 1/Hour

Time Interval Covered
File: 1 Hour
Record: 100 Hz

Portion of Globe Covered
File: Satellite Swath
Record: One CERES footprint

Portion of Atmosphere Covered
File: Satellite Altitude

Table A5. Instrument Earth Scans (IES)

Description	Parameter Number	Units	Range	Elements/ Record	Bits/ Elem	Elem Num
IES						
IES File Header		N/A		1	256	
IES_Start_Info						
Julian Day at Hour Start		day	2449353..2458500	1	32	
Julian Time at Hour Start		day	0..1	1	32	
Colatitude of satellite at IES start		deg	0..180	1	16	
Longitude of satellite at IES start		deg	0..360	1	16	
Number of footprints in IES product		N/A	1..245475	1	32	
Number of orbits		N/A	TBD	1	16	
IES_Footprints is Array[245475] of:						
IES_Footprint_Records						
FOV_Centroid_Info						
TOA_CoLat_&_Long						
Colatitude of CERES FOV at TOA	1	deg	0..180	1	16	1
Longitude of CERES FOV at TOA	2	deg	0..360	1	16	2
Surface_CoLat_&_Long						
Colatitude of CERES FOV at surface	3	deg	0..180	1	16	3
Longitude of CERES FOV at surface	4	deg	0..360	1	16	4
Zenith_Angles						
CERES viewing zenith at TOA	5	deg	0..90	1	16	5
CERES solar zenith at TOA	6	deg	0..180	1	16	6
CERES relative azimuth at TOA	7	deg	0..360	1	16	7
CERES viewing azimuth at TOA wrt North	8	deg	0..360	1	16	8
Miscellaneous_Angles						
Cross-track angle of CERES FOV at TOA	9	deg	-90..90	1	16	9
Along-track angle of CERES FOV at TOA	10	deg	0..360	1	16	10
Clock_&_Cone_Angles						
Cone angle of CERES FOV at satellite	11	deg	0..180	1	16	11
Clock angle of CERES FOV at satellite wrt inertial velocity	12	deg	0..180	1	16	12
Rate of change of cone angle	13	deg sec^{-1}	-100..100	1	16	13
Rate of change of clock angle	14	deg sec^{-1}	-10..10	1	16	14
SC_Velocity						
X component of satellite inertial velocity	15	km sec^{-1}	-10..10	1	16	15
Y component of satellite inertial velocity	16	km sec^{-1}	-10..10	1	16	16
Z component of satellite inertial velocity	17	km sec^{-1}	-10..10	1	16	17
Filtered_Radiances						
CERES total filtered radiance, upwards	18	W m^{-2} sr^{-1}	0..700	1	16	18
CERES shortwave filtered radiance, upwards	19	W m^{-2} sr^{-1}	-10..510	1	16	19
CERES window filtered radiance, upwards	20	W m^{-2} sr^{-1}	0..50	1	16	20
Satellite_&_Sun_Info						
Colatitude of satellite at observation	21	deg	0..180	1	16	21
Longitude of satellite at observation	22	deg	0..360	1	16	22
Radius of satellite from center of Earth at observation	23	km	6000..8000	1	32	23
Colatitude of Sun at observation	24	deg	0..180	1	16	24
Longitude of Sun at observation	25	deg	0..360	1	16	25
Earth-Sun distance	26	AU	0.98 .. 1.02	1	16	26
Observation_References						
Scan sample number	27	N/A	1..660	1	16	27
IES quality flags	28	N/A	0..255	1	16	28
Time of observation	29	day	0..1	1	32	29

Total Meta Bits/File:	400
Total Data Bits/Record:	544
Total Records/File:	245475
Total Data Bits/File:	133538400
Total Bits/File:	133538800

Meteorological, Ozone, and Aerosols (MOA)

The CERES archival product, meteorological, ozone, and aerosols (MOA), is produced by the CERES Regrid Humidity and Temperature Subsystem. Each MOA file contains meteorological data for 1 hour, and is used by several of the CERES subsystems. Data on the MOA are derived from several data sources external to the CERES system, such as NMC, MODIS, SAGE, and various other meteorological satellites. These data arrive anywhere from four times daily to once a month. These data are also horizontally and vertically organized differently from what the CERES system requires. The Regrid Humidity and Temperature Subsystem interpolates these data temporally, horizontally, and vertically to conform with CERES processing requirements.

The MOA contains

- Surface temperature and pressure
- Vertical profiles for up to 38 internal atmospheric levels of temperature, humidity, pressure, and geopotential height
- Column precipitable water
- Vertical ozone profiles for 26 (of the 38) internal atmospheric levels
- Column ozone
- Total column aerosol
- Stratospheric aerosol

The 38 internal atmospheric levels, in hPa, as requested by the CERES clouds and SARB working groups are

Surface	925	775	550	275	125	5
Surface - 10	900	750	500	250	100	1
Surface - 20	875	725	450	225	70	
1000	850	700	400	200	50	
975	825	650	350	175	30	
950	800	600	300	150	10	

Level: 3
Type: Archival
Frequency: 1/Hour

Time Interval Covered
File: 1 hour
Record: 1 hour

Portion of Globe Covered
File: Global
Record: 1.25-deg equal area region

Portion of Atmosphere Covered
File: Surface and Internal

Table A6. Meteorological, Ozone, and Aerosols (MOA)

Description	Parameter Number	Units	Range	Elements/ Record	Bits/ Elem	Elem Num
Meta Data						
Header				1	320	
Regional Data						
Region Number	1	N/A	1..26542	1	16	1
Surface Data						
Surface Temperature	2	K	175..375	1	16	2
Surface Pressure	3	hPa	1100..400	1	16	3
Flag, Source Surface Data	4	N/A	TBD	1	16	4

Table A6. Concluded

Description	Parameter Number	Units	Range	Elements/ Record	Bits/ Elem	Elem Num
Temperature and Humidity Profiles						
Geopotential Height Profiles	5	km	0..50	38	16	5
Pressure Profiles	6	hPa	1100..0	38	16	43
Temperature Profiles	7	K	175..375	38	16	81
Humidity Profiles	8	N/A	0..100	38	16	119
Flag, Source Temp. and Humidity Profiles	9	N/A	TBD	1	16	157
Column Precipitable Water						
Precipitable Water	10	cm	0.001..8.000	1	16	158
Precipitable Water, std	11	cm	TBD	1	16	159
Flag, Source Column Precipitable Water	12	N/A	TBD	1	16	160
Ozone Profile Data						
Ozone Profiles	13	$g\ kg^{-1}$	0.00002..0.02	26	16	161
Flag, Source Ozone Profile Data	14	N/A	TBD	1	16	187
Column Ozone						
Column Ozone	15	du	200..500	1	16	188
Flag, Source Column Ozone	16	N/A	TBD	1	16	189
Total Column Aerosol						
Aerosol Mass Loading, Total Column	17	$g\ m^{-2}$	TBD	1	16	190
Flag, Source Aerosol Mass Loading, Total Column	18	N/A	TBD	1	16	191
Optical Depth, Total Column	19	N/A	0.0..2.0	1	16	192
Flag, Source Optical Depth, Total Column	20	N/A	TBD	1	16	193
Asymmetry Factor, Total Column	21	N/A	0.0..1.0	1	16	194
Flag, Source Asymmetry Factor, Total Column	22	N/A	TBD	1	16	195
Single Scattering Albedo, Total Column	23	N/A	0.0..1.0	1	16	196
Flag, Source Single Scattering Albedo, Total Column	24	N/A	TBD	1	16	197
Effective Particle Size, Total Column	25	µm	0.0..20.0	1	16	198
Flag, Source Effective Particle Size, Total Column	26	N/A	TBD	1	16	199
Mean Aerosol Layer Temperature, Total Column	27	K	150..280	1	16	200
Flag, Source Mean Aerosol Layer Temperature, Total Column	28	N/A	TBD	1	16	201
Stratospheric Aerosol						
Optical Depth, Stratosphere	29	N/A	0.0..0.5	1	16	202
Asymmetry Factor, Stratosphere	30	N/A	0.0..1.0	1	16	203
Single Scattering Albedo, Stratosphere	31	N/A	0.0..1.0	1	16	204
Effective Particle Size, Stratosphere	32	µm	0.0..10.0	1	16	205
Mean Aerosol Layer Temperature, Stratosphere	33	K	150..280	1	16	206
Flag, Source Stratospheric Aerosol	34	N/A	TBD	1	16	207

Total Meta Bits/File:	320
Total Data Bits/Record:	3312
Total Records/File:	26542
Total Data Bits/File:	87907104
Total Bits/File:	87907424

Microwave Liquid Water Path (MWP)

The microwave liquid water path (MWP) product is a daily, level 2 product. The product con-tains a product header followed by the microwave water path parameter values, which are total atmospheric column integrated. The TRMM microwave imager (TMI) data swath on TRMM is approximately 700 km, while the multifrequency imaging microwave radiometer (MIMR) data swath used for EOS is approximately 1 400 km. The FOV of MIMR and TMI is approximately 20 km at nadir, so an estimate of the number of MIMR pixels in a scan line is about 75 and the number of scan lines in a day is about 250 000.

The MWP Product is a non-EOS ancillary product, external to the CERES processing system, that the CERES project plans to keep in the LaRC DAAC for reprocessing.

Level: 2
Type: Ancillary
Frequency: 1/Day

Portion of Globe Covered
File: Global
Record: Swath

Time Interval Covered
File: 24 Hours
Record: One scan

Portion of Atmosphere Covered
File: Total atmospheric column

Table A7. Microwave Liquid Water Path (MWP)

Description	Parameter Number	Units	Range	Elements/ Record	Bits/ Elem	Elem Num
MWP						
MWP header record - TBD		N/A	N/A	1	2048	
Records_MWP is Array[25000] of:						
Scan_lines_MWP						
Pixels_MWP is Array[75] of:						
H2OC_Path						
Time of observation	1	day	0..1	75	32	1
Latitude of MWP pixel	2	deg	-90 .. 90	75	32	76
Longitude of MWP pixel	3	deg	-90 .. 90	75	32	151
Microwave water path data	4	kg m^{-2}	TBD	75	16	226

Total Meta Bits/File:	2048
Total Data Bits/Record:	8400
Total Records/File:	25000
Total Data Bits/File:	210000000
Total Bits/File :	210002048

Surface Map (SURFMAP)

The surface map and properties (SURFMAP) product is a composite product of different types of surface conditions, arranged on a global 10 km by 10 km equal-area grid. The individual products received from different non-EOS sources are

SURFMAP(DEM)	Digital elevation map
SURFMAP(H2O)	Water map
SURFMAP(ICE)	Ice map
SURFMAP(SNOW)	Snow map
SURFMAP(VEGE)	Vegetation map

The remaining surface data are compiled by the CERES science team from various clear-sky models into the SURFMAP(STD) product.

SURFMAP(STD)	Science thermophysical data

The STD product consists of

Surface type indicator
Broadband shortwave surface ADM type
Visible albedo for collimated, overhead sun illumination
Spectral emissivity from 3.7-micron channel imager data
Spectral emissivity from 11.0-micron channel imager data

The surface type indicator specifies which of the surface conditions best describes the grid cell (land, water, snow, or ice). Snow/ice takes precedence over land/water.

Each of the above products contain a product header and parameters for each 10 km by 10 km equal area grid cell. The SURFMAP is updated at different frequencies, depending on the type of data. For example, the snow and ice map are updated weekly, whereas the elevation map may be used for the life of the mission.

The SURFMAP product will be retained at the LaRC DAAC permanently. EOSDIS may provide the data for some of the required surface conditions, which the CERES software would access through the product generation system toolkit.

Level: 3
Type: Ancillary
Frequency: 1/Week

Portion of Globe Covered
File: Entire globe
Record: 10 km equal area grid

Time Interval Covered
File: 1 Week
Record: 1 Week

Portion of Atmosphere Covered
File: Surface

Table A8. Surface Map (SURFMAP)

Description	Parameter Number	Units	Range	Elements/ Record	Bits/ Elem	Elem Num
SURFMAP						
SURFMAP_Composite_Product is Array[1] of:						
SURFMAP_Individual_Products						
DEM						
Header record		N/A	N/A	1	2048	
Record_DEM is Array[4341600] of:						
Digital Elevation Model	1	km	-12..10	4341600	16	1
H2O						
Header record		N/A	N/A	1	2048	
Record_H2O is Array[4341600] of:						
Water map	2	percent	0 .. 100	4341600	16	4341601
ICE						
Header record		N/A	N/A	1	2048	
Record_ICE is Array[4341600] of:						
Ice map	3	percent	0 .. 100	4341600	16	8683201
SNOW						
Header record		N/A	N/A	1	2048	
Record_SNOW is Array[4341600] of:						
Snow map	4	percent	0 .. 100	4341600	16	13024801
VEGE						
Header record		N/A	N/A	1	2048	
Record_VEGE is Array[4341600] of:						
Vegetation map	5	TBD	TBD	4341600	16	17366401
STD						
Header record		N/A	N/A	1	2048	
Record_STD is Array[4341600] of:						
Science_Thermophysical_Data						
Surface type indicator for each grid	6	N/A	1 .. 13	4341600	16	21708001
Broadband shortwave surface ADM type	7	N/A	TBD	4341600	16	26049601
Visible albedo for collimated, overhead sun illumination	8	N/A	0 .. 1	4341600	16	30391201
Spectral emissivity at 3.7 micrometers	9	N/A	TBD	4341600	16	34732801
Spectral emissivity at 11 micrometers	10	N/A	TBD	4341600	16	39074401

Total Meta Bits/File:	12288
Total Data Bits/Record:	694656000
Total Records/File:	1
Total Data Bits/File:	694656000
Total Bits/File :	694668288

Appendix B

Output Data Products

Determine Cloud Properties, TOA and Surface Fluxes (Subsystem 4.0)

This appendix describes the data products which are produced by the algorithms in this subsystem. Table B-1 below summarizes these products, listing the CERES and EOSDIS product codes or abbreviations, a short product name, the product type, the production frequency, and volume estimates for each individual product as well as a complete data month of production. The product types are defined as follows:

Archival products:	Assumed to be permanently stored by EOSDIS
Internal products:	Temporary storage by EOSDIS (days to years)

The following pages describe each product. An introductory page provides an overall description of the product and specifies the temporal and spatial coverage. The table which follows the introductory page briefly describes every parameter which is contained in the product. Each product may be thought of as metadata followed by data records. The metadata (or header data) is not well-defined yet and is included mainly as a placeholder. The description of parameters which are present in each data record includes parameter number (a unique number for each distinct parameter), units, dynamic range, the number of elements per record, an estimate of the number of bits required to represent each parameter, and an element number (a unique number for each instance of every parameter). A summary at the bottom of each table shows the current estimated sizes of metadata, each data record, and the total data product. A more detailed description of each data product will be contained in a user's guide to be published before the first CERES launch.

Table B1. Output Products Summary

Product Code		Name	Type	Frequency	Size, MB	Monthly Size, MB
CERES	EOSDIS					
CRH_DB	CERX03	Clear reflectance history	archival	Every 10 days	91.1	91
SSF	CER11	Single satellite footprint, and surface flux, clouds	archival	1/hour	154.0	114576

Clear Reflectance History (CRH_DB)

The clear reflectance/temperature history (CRH) data are organized on a global equal-area grid that is approximately 10 km by 10 km. The data coverage is 24 hours, and is updated twice a day if clear-sky conditions exist for the particular grid cell. The data product consists of a product header followed by fixed-length records organized according to the grid pattern. The parameters are derived from cloud imager measurements by subsystem 4. The CRH_DB product is the same structure for both MODIS values and VIRS values. There is a source indication on the header record.

The CRH_DB is used in subsystem 11 to update the CRH archival product about every 10 days. The CRH product retains clear-sky information for the life of the mission, whereas the CRH_DB contains only the most recent 10 day clear-sky data.

Level: 3
Type: Internal
Frequency: Every 10 Days

Time Interval Covered
File: 10 Days
Record: 2/Day

Portion of Globe Covered
File: Entire Globe
Record: 10km by 10km grid

Portion of Atmosphere Covered
File: Surface Reference

Table B2. Clear Reflectance History (CRH_DB)

Description	Parameter Number	Units	Range	Elements/ Record	Bits/ Elem	Elem Num
CRH_DB						
CRH header record		N/A	N/A	1	2048	
Record_CRH_DB is Array[4341600] of:						
Grid_CRH_DB						
Day of observation	1	day	Mission Life	1	32	1
Time of observation	2	day	0..1	1	32	2
Visible albedo for collimated, overhead sun illumination	3	N/A	0 .. 1	1	16	3
Temperature derived from 3.7 µm imager channel	4	K	TBD	1	16	4
Temperature derived from 11 µm imager channel	5	K	TBD	1	16	5
Solar zenith angle from imager	6	deg	0 .. 90	1	16	6
Mean imager viewing zenith over CERES FOV	7	deg	0 .. 90	1	16	7
Mean imager relative aziumth angle over CERES FOV	8	deg	0 .. 360	1	16	8
Narrowband ADM Type	9	N/A	TBD	1	16	9

Total Meta Bits/File:	2048
Total Data Bits/Record:	176
Total Records/File:	4341600
Total Data Bits/File:	764121600
Total Bits/File :	764123648

Single Satellite Footprint, TOA and Surface Flux, Clouds (SSF)

The single satellite flux and cloud swaths (SSF) is produced from the cloud identification, inversion, and surface processing for CERES. Each SSF covers a single hour swath from a single CERES instrument mounted on one satellite. The product has a product header and multiple records of approximately 125 parameters or 315 elements for each pixel.

The major categories of data output on the SSF are

- CERES footprint geometry and CERES viewing angles
- CERES footprint radiance and flux (TOA and Surface)
- CERES footprint cloud statistics and imager viewing angles
- CERES footprint clear area statistics
- CERES footprint cloudy area statistics for each of four cloud height categories
  - Visible optical depth (mean and standard deviation)
  - Infrared emissivity (mean and standard deviation)
  - Liquid water path (mean and standard deviation)
  - Ice water path (mean and standard deviation)
  - Cloud top pressure (mean and standard deviation)
  - Cloud effective pressure (mean and standard deviation)
  - Cloud effective temperature (mean and standard deviation)
  - Cloud effective height (mean and standard deviation)
  - Cloud bottom pressure (mean and standard deviation)
  - Water particle radius (mean and standard deviation)
  - Ice particle radius (mean and standard deviation)

Particle phase (mean and standard deviation)
Vertical aspect ratio (mean and standard deviation)
Visible optical depth/IR emissivity (13 percentiles)
CERES footprint cloud overlap conditions (11 conditions)

The SSF is an archival product that will be run daily in validation mode starting with the TRMM launch until sufficient data have been collected and analyzed to produce a production quality set of CERES angular distrubution models (ADM). It is estimated that at TRMM launch plus 18 months, the SSF product will be produced on a routine basis and will be archived within EOSDIS for distribution. The inversion process will be rerun starting from the TRMM launch and a new SSF produced, in which case, only the TOA fluxes and surface parameters will be replaced in the inversion rerun process. If the cloud algorithms are rerun, the SSF product itself will be input into the cloud identification process in order to retrieve the CERES radiance and location data input data needed.

Level: 2
Type: Archival
Frequency: 1/Hour

Portion of Globe Covered
File: Satellite Swath
Record: One Footprint

Time Interval Covered
File: 1 Hour
Record: 1/100 Second

Portion of Atmosphere Covered
File: Surface to TOA

Table B3. Single Satellite Footprint, TOA and Surface Flux, Clouds (SSF)

Description	Parameter Number	Units	Range	Elements/ Record	Bits/ Elem	Elem Num
SSF						
SSF_Header						
Julian Day at Hour Start		day	2449353..2458500	1	32	
Julian Time at Hour Start		day	0..1	1	32	
Character name of satellite		N/A		1	16	
Number of orbits		N/A	TBD	1	16	
Name of high resolution imager instrument		N/A	N/A	1	16	
Number of footprints in IES product		count	1..245475	1	32	
Number of imager channels used		N/A	1 .. 11	1	16	
WavLen_Array is Array[11] of:						
Central wavelengths of imager channels		µm	0.4 .. 15.0	11	16	
SSF_Record is Array[245475] of:						
SSF_Footprints						
Footprint_Geometry						
Time_and_Position						
Time of observation	1	day	0..1	1	32	1
Earth-Sun distance	2	AU	0.98 .. 1.02	1	16	2
Radius of satellite from center of Earth at observation	3	km	6000..8000	1	32	3
Colatitude of satellite at observation	4	deg	0..180	1	16	4
Longitude of satellite at observation	5	deg	0..360	1	16	5
Colatitude of Sun at observation	6	deg	0..180	1	16	6
Longitude of Sun at observation	7	deg	0..360	1	16	7
Colatitude of CERES FOV at TOA	8	deg	0..180	1	16	8
Longitude of CERES FOV at TOA	9	deg	0..360	1	16	9
Colatitude of CERES FOV at surface	10	deg	0..180	1	16	10
Longitude of CERES FOV at surface	11	deg	0..360	1	16	11
Scan sample number	12	N/A	1..660	1	16	12
Cone angle of CERES FOV at satellite	13	deg	0..180	1	16	13
Clock angle of CERES FOV at satellite wrt inertial velocity	14	deg	0..180	1	16	14
Rate of change of cone angle	15	deg sec^{-1}	-100..100	1	16	15
Rate of change of clock angle	16	deg sec^{-1}	-10..10	1	16	16
Along-track angle of CERES FOV at TOA	17	deg	0..360	1	16	17
Cross-track angle of CERES FOV at TOA	18	deg	-90..90	1	16	18

Table B3. Continued

Description	Parameter Number	Units	Range	Elements/ Record	Bits/ Elem	Elem Num
X component of satellite inertial velocity	19	km sec^{-1}	-10..10	1	16	19
Y component of satellite inertial velocity	20	km sec^{-1}	-10..10	1	16	20
Z component of satellite inertial velocity	21	km sec^{-1}	-10..10	1	16	21
CERES_Viewing_Angles						
CERES viewing zenith at TOA	22	deg	0..90	1	16	22
CERES solar zenith at TOA	23	deg	0..180	1	16	23
CERES relative azimuth at TOA	24	deg	0..360	1	16	24
CERES viewing azimuth at TOA wrt North	25	deg	0..360	1	16	25
Surface_Map_Parameters						
Mean altitude of surface above sea level	26	km	-12 .. 10	1	16	26
LandTyps is Array[10] of:						
Area fraction of land types in percent	27	N/A	0 .. 100	10	16	27
SeaTyps is Array[3] of:						
Area fraction of sea types in percent	28	N/A	0 .. 100	3	16	37
Scene_Type						
CERES clear sky or full sky indicator	29	N/A	N/A	1	16	40
CERES scene type for Inversion process	30	N/A	0 .. 200	1	16	41
Footprint_Radiation						
CERES_Filtered_Radiances						
CERES total filtered radiance, upwards	31	$W\text{-}m^{-2}sr^{-1}$	0..700	1	16	42
CERES shortwave filtered radiance, upwards	32	$W\text{-}m^{-2}sr^{-1}$	-10..510	1	16	43
CERES window-filtered radiance, upwards	33	$W\text{-}m^{-2}sr^{-1}$	0..50	1	16	44
Quality flag for total radiance value	34	N/A	N/A	1	16	45
Quality flag for SW radiance value	35	N/A	N/A	1	16	46
Quality flag for window radiance value	36	N/A	N/A	1	16	47
CERES_Unfiltered_Radiances						
CERES shortwave radiance, upwards	37	$W\text{-}m^{-2}sr^{-1}$	-10..510	1	16	48
CERES longwave radiance, upwards	38	$W\text{-}m^{-2}sr^{-1}$	0..200	1	16	49
CERES window radiance, upwards	39	$W\text{-}m^{-2}sr^{-1}$	0..50	1	16	50
TOA_and_Surface_Flux						
CERES shortwave flux at TOA, upwards	40	$W\text{-}m^{-2}$	0..1400	1	16	51
CERES longwave flux at TOA, upwards	41	$W\text{-}m^{-2}$	0..500	1	16	52
CERES window flux at TOA, upwards	42	$W\text{-}m^{-2}$	10..400	1	16	53
CERES shortwave flux at surface, downwards	43	$W\text{-}m^{-2}$	0..1400	1	16	54
CERES longwave flux at surface, downwards	44	$W\text{-}m^{-2}$	0..500	1	16	55
CERES net shortwave flux at surface	45	$W\text{-}m^{-2}$	0..1400	1	16	56
CERES net longwave flux at surface	46	$W\text{-}m^{-2}$	0..500	1	16	57
CERES surface emissivity	47	N/A	0..1	1	16	58
Photosynthetically active radiation at surface	48	$W\text{-}m^{-2}$	0..780	1	16	59
Direct/diffuse ratio at the surface	49	TBD	0..30	1	16	60
Full_Footprint_Area						
Mean imager viewing zenith over CERES FOV	50	deg	0 .. 90	1	16	61
Mean imager relative aziumth angle over CERES FOV	51	deg	0 .. 360	1	16	62
Number of cloud height categories	52	N/A	-1 .. 4	1	16	63
Number of imager pixels in CERES FOV	53	N/A	0 .. 9000	1	16	64
BDRF_Image is Array[11] of:						
Bidirectional reflectance or brightness temperature	54	TBD	TBD	11	16	65
Precipitable water	55	cm	0.001 .. 8	1	16	76
5th percentile of 0.6-µm imager radiances over CERES FOV	56	$W\text{-}m^{-2}sr^{-1}\mu m^{-1}$	TBD	1	16	77
Mean of 0.6 µm imager radiances over CERES FOV	57	$W\text{-}m^{-2}sr^{-1}\mu m^{-1}$	TBD	1	16	78
95th percentile of 0.6-µm imager radiances over CERES FOV	58	$W\text{-}m^{-2}sr^{-1}\mu m^{-1}$	TBD	1	16	79
5th percentile of 3.7-µm imager radiances over CERES FOV	59	$W\text{-}m^{-2}sr^{-1}\mu m^{-1}$	TBD	1	16	80
Mean of the 3.7-µm imager radiances over CERES FOV	60	$W\text{-}m^{-2}sr^{-1}\mu m^{-1}$	TBD	1	16	81
95th percentile of 3.7-µm imager radiances over CERES FOV	61	$W\text{-}m^{-2}sr^{-1}\mu m^{-1}$	TBD	1	16	82
5th percentile of 11-µm imager radiances over CERES FOV	62	$W\text{-}m^{-2}sr^{-1}\mu m^{-1}$	TBD	1	16	83
Mean of the 11-µm imager radiances over CERES FOV	63	$W\text{-}m^{-2}sr^{-1}\mu m^{-1}$	TBD	1	16	84

Table B3. Continued

Description	Parameter Number	Units	Range	Elements/ Record	Bits/ Elem	Elem Num
95th percentile of 11-μm imager radiances over CERES FOV	64	$W\text{-}m^{-2}sr^{-1}\mu m^{-1}$	TBD	1	16	85
Notes on general procedures	65	N/A	TBD	1	16	86
Texture algorithm flag	66	N/A	TBD	1	16	87
Multilevel cloud algorithm flag	67	N/A	TBD	1	16	88
Spatial coherence algorithm flag	68	N/A	TBD	1	16	89
Infrared sounder algorithm flag	69	N/A	TBD	1	16	90
Threshhold algorithm flag	70	N/A	TBD	1	16	91
Visible optical depth algorithm flag	71	N/A	TBD	1	16	92
Infrared emissivity algorithm flag	72	N/A	TBD	1	16	93
Cloud particle size algorithm flag	73	N/A	TBD	1	16	94
Cloud water path algorithm flag	74	N/A	TBD	1	16	95
Clear_Footprint_Area						
Mean of 0.6-μm imager radiances over clear area	75	$W\text{-}m^{-2}sr^{-1}\mu m^{-1}$	TBD	1	16	96
Stddev of the 0.6-μm imager radiances over clear area	76	$W\text{-}m^{-2}sr^{-1}\mu m^{-1}$	TBD	1	16	97
Mean of the 3.7-μm imager radiances over clear area	77	$W\text{-}m^{-2}sr^{-1}\mu m^{-1}$	TBD	1	16	98
Stddev of 3.7-μm imager radiances over clear area	78	$W\text{-}m^{-2}sr^{-1}\mu m^{-1}$	TBD	1	16	99
Mean of the 11-μm imager radiances over clear area	79	$W\text{-}m^{-2}sr^{-1}\mu m^{-1}$	TBD	1	16	100
Stddev of the 11-μm imager radiances over clear area	80	$W\text{-}m^{-2}sr^{-1}\mu m^{-1}$	TBD	1	16	101
Stratospheric aerosol visible optical depth in clear area	81	N/A	0 .. 0.5	1	16	102
Stratospheric aerosol effective radius in clear area	82	μm	0 .. 10	1	16	103
Total aerosol visible optical depth in clear area	83	N/A	0 .. 2	1	16	104
Total aerosol effective radius in clear area	84	μm	0 .. 20	1	16	105
Cloudy_Footprint_Area is Array[4] of:						
Cloud_Cat_Arrays						
Number of imager pixels for cloud category	85	N/A	0 .. 9000	4	16	106
Number of overcast pixels for cloud category	86	N/A	0 .. 9000	4	16	110
Cloud category weighted area fraction	87	N/A	0 .. 1	4	16	114
Cloud category weighted overcast fraction	88	N/A	0 .. 1	4	16	118
Cloud category weighted broken fraction	89	N/A	0 .. 1	4	16	122
Mean of 0.6-μm imager radiances for cloud category	90	$W\text{-}m^{-2}sr^{-1}\mu m^{-1}$	TBD	4	16	126
Stddev of 0.6-μm imager radiance for cloud category	91	$W\text{-}m^{-2}sr^{-1}\mu m^{-1}$	TBD	4	16	130
Mean of 3.7-μm imager radiances for cloud category	92	$W\text{-}m^{-2}sr^{-1}\mu m^{-1}$	TBD	4	16	134
Stddev of 3.7-μm imager radiances for cloud category	93	$W\text{-}m^{-2}sr^{-1}\mu m^{-1}$	TBD	4	16	138
Mean of 11-μm imager radiances for cloud category	94	$W\text{-}m^{-2}sr^{-1}\mu m^{-1}$	TBD	4	16	142
Stddev of 11-μm imager radiances for cloud category	95	$W\text{-}m^{-2}sr^{-1}\mu m^{-1}$	TBD	4	16	146
Mean cloud visible optical depth for cloud category	96	N/A	0 .. 400	4	16	150
Stddev of visible optical depth for cloud category	97	N/A	TBD	4	16	154
Mean cloud infrared emissivity for cloud category	98	N/A	0 .. 1	4	16	158
Stddev of cloud infrared emissivity for cloud category	99	N/A	TBD	4	16	162
Mean liquid water path for cloud category	100	$kg\ m^{-2}$	TBD	4	16	166
Stddev of liquid water path for cloud category	101	$kg\ m^{-2}$	TBD	4	16	170
Mean ice water path for cloud category	102	$kg\ m^{-2}$	TBD	4	16	174
Stdev of ice water path for cloud category	103	$kg\ m^{-2}$	TBD	4	16	178
Mean cloud top pressure for cloud category	104	hPa	0 .. 1100	4	16	182
Stddev of cloud top pressure for cloud category	105	hPa	TBD	4	16	186
Mean cloud effective pressure for cloud category	106	hPa	0 .. 1100	4	16	190
Stddev of cloud effective pressure for cloud category	107	hPa	TBD	4	16	194
Mean cloud effective temperature for cloud category	108	K	100 .. 350	4	16	198
Stddev of cloud effective temperature for cloud category	109	K	TBD	4	16	202
Mean cloud effective height for cloud category	110	km	0 .. 20	4	16	206
Stddev of cloud effective height for cloud category	111	km	TBD	4	16	210
Mean cloud bottom pressure for cloud category	112	hPa	0 .. 1100	4	16	214
Stddev of cloud bottom pressure for cloud category	113	hPa	TBD	4	16	218
Mean water particle radius for cloud category	114	TBD	TBD	4	16	222
Stddev of water particle radius for cloud category	115	TBD	TBD	4	16	226
Mean ice particle radius for cloud category	116	TBD	TBD	4	16	230

Table B3. Concluded

Description	Parameter Number	Units	Range	Elements/ Record	Bits/ Elem	Elem Num
Stddev of ice particle radius for cloud category	117	TBD	TBD	4	16	234
Mean cloud particle phase for cloud category	118	N/A	0 .. 1	4	16	238
Stddev of cloud particle phase for cloud category	119	N/A	0 .. 1	4	16	242
Mean vertical aspect ratio for cloud category	120	N/A	0 .. 1	4	16	246
Stddev of vertical aspect ratio for cloud category	121	N/A	TBD	4	16	250
Optical_Depth_Percentile is Array[13] of:						
Percentiles of visible optical depth/IR emissivity for cloud category	122	N/A	TBD	52	16	254
Overlap_Footprint_Area is Array[11] of:						
Overlap_Conditions						
Number of imager pixels for overlap condition	123	N/A	0 .. 9000	11	16	306
Overlap condition weighted area fraction	124	N/A	0 .. 1	11	16	317

Total Meta Bits/File:	336
Total Data Bits/Record:	5264
Total Records/File:	245475
Total Data Bits/File:	1292180400
Total Bits/File :	1292180736

4.0.9. References

Arking, A.; and Childs, J. D. 1985: Retrieval of Cloud Cover Parameters From Multispectral Satellite. *J. Climat. & Appl. Meteorol.*, vol. 24, pp. 322–333.

Baum, Bryan A.; Arduini, Robert F.; Wielicki, Bruce A.; Minnis, Patrick; and Si-Chee, Tsay 1994: Multilevel Cloud Retrieval Using Multispectral HIRS and AVHRR Data: Nighttime Oceanic Analysis. *J. Geophys. Res.*, vol. 99, no. D3, pp. 5499–5514.

Cahalan, Robert F.; Ridgway, William; Wiscombe, Warren J.; Gollmer, Steven; and Harshvardhan 1994: Independent Pixel and Monte Carlo Estimates of Stratocumulus Albedo. *J. Atmos. Sci.*, vol. 51, no. 24, pp. 3776–3790.

Coakley, J. A., Jr.; and Bretherton, F. P. 1982: Cloud Cover From High-Resolution Scanner Data: Detecting and Allowing for Partially Filled Fields of View. *J. Geophys. Res.*, vol. 87, pp. 4917–4932.

Coakley, J. A., Jr.; and Davies, R. 1986: The Effect of Cloud Sides on Reflected Solar Radiation as Deduced from Satellite Observations. *J. Atmos. Sci.*, vol. 43, pp. 1025–1035.

Coakley, James A., Jr.; Bernstein, Robert L.; and Durkee, Philip A. 1987: Effect of Ship-Stack Effluents on Cloud Reflectivity. *Science*, vol. 237, pp. 1020–1022.

Greenwald, Thomas J.; Stephens, Graeme, L.; Vonder Haar, Thomas H.; and Jackson, Darren L. 1993: A Physical Retrieval of Cloud Liquid Water Over the Global Oceans Using Special Sensor Microwave/Imager (SSM/I) Observations. *J. Geophys. Res.*, vol. 98, no. D10, pp. 18471–18488.

Hahn, C. J.; Warren, S. G.; London, J.; Chervin, R. M; and Jenne, R. 1982: *Atlas of Simultaneous Occurrence of Different Cloud Types Over the Ocean*. NCAR TN-201.

Harshvardhan; Ginger, K.; and Wielicki, B. A. 1994: The Interpretation of Remotely Sensed Cloud Properties From a Model Parameterization Perspective. *Eighth Conference on Atmospheric Radiation*, pp. 443–445.

Jacobowitz, H.; Soule, H. V.; Kyle, H. L.; and House, F. B. 1984: The Earth Radiation Budget (ERB) Experiment—An Overview. *J. Geophys. Res.*, vol. 89, pp. 5021–5038.

King, M. D.; Kaufman, Y. J.; Menzel, W. P.; and Tanre, D. 1992: Remote Sensing of Cloud, Aerosol, and Water Vapor Properties from the Moderate Resolution Imaging Spectrometer (MODIS). *IEEE Trans. Geosci. & Remote Sens.*, vol. 30, no. 1, pp. 2–27.

Lin, X.; and Coakley, J. A., Jr. 1993: Retrieval of Properties for Semitransparent Clouds From Multispectral Infrared Imagery Data. *J. Geophys. Res.*, vol. 98, pp. 18,501–18,514.

Luo, G.; Lin, X.; and Coakley, J. A. 1994: 11-μm Emissivities and Droplet Radii for Marine Stratocumulus. *J. Geophys. Res.*, vol. 99, pp. 3685–3698.

Minnis, Patrick; Heck, Patrick W.; and Young, David 1993: Inference of Cirrus Cloud Properties Using Satellite-Observed and Infrared Radiances. Part II: Verification of Theoretical Cirrus Radiative Properties. *J. Atmos. Sci.*, vol. 50, no. 9, p. 1322.

Nagarajarao, C. R., ed. 1993: *Degradation of the Visible and Near-Infrared Channels of the Advanced Very High Resolution Radiometer on the NOAA-9 Spacecraft—Assessment and Recommendations for Corrections*. NOAA-TR-NESDIS-70.

Payette, F. 1989: Application of a Sampling Strategy for the ERBE Scanner Data. M.S. Thesis, McGill Univ.

Rossow, William B. 1989: Measuring Cloud Properties From Space—A Review. *J. Climat.*, vol. 2, pp. 201–213.

Rossow, William B.; Garder, Leonid, C.; Lu, Pei-Jane; and Walker, Alison 1992: *International Satellite Cloud Climatology Project (ISCCP): Documentation of Cloud Data*. World Meteorol. Org.

Staylor, W. Frank 1990: Degradation Rates of the AVHRR Visible Channel for the NOAA 6, 7, and 9 Spacecraft. *J. Atmos. & Ocean. Technol.*, vol. 7, pp. 411–423.

Stackhouse, P. W.; and Stephens, G. L. 1994: Investigation of the Effects of Macrophysical and Microphysical Properties of Cirrus Clouds on the Retrieval of Optical Properties—Result from FIRE II. *Eighth Conference on Atmospheric Radiation*, pp. 225–227.

Stephens, Graeme L. 1988: Radiative Transfer Through Arbitrarily Shaped Optical Media. II—Group Theory and Simple Closures. *J. Atmos. Sci.*, vol. 45, pp. 1818–1848.

Stephens, G. L.; Paltridge, G. W.; and Platt, C. M. R. 1978: Radiation Profiles in Extended Water Clouds. III—Observation. *J. Atmos. Sci.*, vol. 35, pp. 2133–2141.

Stowe, L. L.; Wellemeyer, C. G.; Eck, T. F.; and Yeh, H. Y. M.; and Nimbus-7 Cloud Data Processing Team 1988: Nimbus-7 Global Cloud Climatology. I—Algorithms and Validation. *J. Climat*., vol. 1, no. 5, pp. 445–470.

Suttles, J. T.; Green, R. N.; Minnis, P.; Smith, G. L.; Staylor, W. F.; Wielicki, B. A.; Walker, I. J.; Young, D. F.; Taylor, V. R.; and Stowe, L. L. 1988: *Angular Radiation Models for Earth-Atmosphere System. Volume I: Shortwave Radiation*. NASA RP-1184.

Suttles, John T.; Wielicki, Bruce A.; and Vemury, Sastri 1992: Top-of-Atmosphere Radiative Fluxes—Validation of ERBE Scanner Inversion Algorithm Using Nimbus-7 ERB Data. *J. Appl. Meteorol.*, vol. 31, no. 7, pp. 784–796.

Takano, Yoshihide; and Liou, Kuo-Nan 1989: Solar Radiative Transfer in Cirrus Clouds. I—Single-Scattering and Optical Properties of Hexagonal Ice Crystals. *J. Atmos. Sci.*, vol. 46, pp. 3–36.

Tian, Lin; and Curry, Judith A. 1989: Cloud Overlap Statistics. *J. Geophys. Res.*, vol. 94, pp. 9925–9935.

Taylor, V. Ray; and Stowe, Larry L. 1984: Reflectance Characteristics of Uniform Earth and Cloud Surfaces Derived from NIMBUS 7 ERB. *J. Geophys. Res.*, vol. 89, no. D4, pp. 4987–4996.

Warren, S. G.; Hahn, C. J.; and London, J. 1985: Simultaneous Occurrence of Different Cloud Types. *J. Climat. and Appl. Meteorol.*, vol. 24, pp. 658–667.

Welch, Ronald M.; Cox, Stephen K.; and Davis, John M. 1980: Solar Radiation and Clouds. *Meteorol. Monogr*., vol. 17, no. 39.

Wielicki, Bruce A.; and Green, Richard N. 1989: Cloud Identification for ERBE Radiative Flux Retrieval. *J. Appl. Meteorol.*, vol. 28, pp. 1133–1146.

Wielicki, Bruce A.; and Barkstrom, Bruce R. 1991: Clouds and the Earth's Radiant Energy System (CERES)—An Earth Observing System Experiment. *Second Symposium on Global Change Studies—Preprints*, American Meteorol. Soc., pp. 11–16.

Wielicki, Bruce A.; and Parker, Lindsay 1992: On the Determination of Cloud Cover from Satellite Sensors—The Effect of Sensor Spatial Resolution. *J. Geophys. Res.*, vol. 97, no. D12, pp. 12799–12823.

Wielicki, B. A.; and Welch, R. M. 1986: Cumulus Cloud Properties Derived Using Landsat Satellite Data. *J. Climat. & Appl. Meteorol.*, vol. 25, pp. 261–276.

Ye, Qian 1993: The Spatial-Scale Dependence of the Observed Anisotropy of Reflected and Emitted Radiation. PH.D Diss., Ohio State Univ.